Engineering Reports

WILEY

Engineering Reports Open Access

RESEARCH ARTICLE OPEN ACCESS

Smart Mosquito-Nets: A Natural Approach to Controlling Malaria Using Larvicidal Plant Extracts and Internet of Things

Juliet Onyinye Nwigwe[1] | Kennedy Chinedu Okafor[1,2,3,4,5] | Ogonna Christiana Ani[6] | Titus Ifeanyi Chinebu[1] | Okafor Ijeoma Peace[7] | Omowunmi Mary Longe[3] | Kelvin Anoh[4]

[1]Department of Applied Sciences, Federal University of Allied Health Sciences, Enugu, Nigeria | [2]Imperial College Business School, Imperial College London, London, UK | [3]Department of Electrical and Electronic Engineering Science, University of Johannesburg, Johannesburg, South Africa | [4]Center for Future Technologies, University of Chichester, Bognor Regis, UK | [5]Department of Engineering, Manchester Metropolitan University, Manchester, UK | [6]Department of Applied Biology, Ebonyi State University, Abakaliki, Nigeria | [7]Department of Public Health, Cardiff Metropolitan University, Cardiff, UK

Correspondence: Kennedy Chinedu Okafor (kennedy.okafor@mmu.ac.uk)

Received: 23 December 2024 | **Revised:** 12 August 2025 | **Accepted:** 11 September 2025

Funding: This work was supported by Institute of Electrical and Electronics Engineers (IEEE), USA.

Keywords: compartmental modeling | elastic compute simulation | fractal fractional order derivatives | integer order model | internet of things | larvicidal plant extracts

ABSTRACT

Malaria mosquitoes, Anopheles, are well-known for carrying and spreading the malaria pathogens, known as Plasmodium. The public health challenge it brings has remained a global health challenge, of which the most robust control measures include mosquito-treated nets and electronic mosquito killer lamps. Due to health and cost problems, for example, in developing countries, these methods are not suitable for controlling mosquitoes and their plasmodiumic pathogens. In this study, we propose the use of two natural plant (e.g., *Petiveria alliacea* and *Hyptis suavolens* leaf) extracts that are cheap, ubiquitous, and effective for the control of mosquitoes, especially in temperate regions such as sub-Saharan Africa. On top of that, the study uses memory, non-locality, and fractal properties of fractal-fractional derivatives from compartmental modeling to capture susceptibility of infected persons, wider coverage, and heterogeneous breeding of mosquitoes, respectively, to evaluate the effectiveness of the two leaf extracts as natural larvicides against *Anopheles* mosquitoes. To measure the effectiveness of the two plant extracts in controlling malaria, this study develops a basic reproduction number model of Anopheles mosquitoes and evaluates the endemic points of the model. Comparing the results of larvicidal control with those of mosquito-treated nets, the proposed larvicidal control achieved 94.86% efficacy when applied alone and 96.83% efficacy when combined with mosquito nets, each outperforming mosquito nets (83.33%). These findings position compartmental fractal fractional-order modeling as an innovative tool for bioinformatic disease vector control. The study also presents a smart mosquito-net model where data collected from the host nodes on the performance of larvicides in mosquito and malaria control are transmitted via the Internet of Things infrastructure to the edge and cloud servers for computation, processing, artificial intelligence analytics, and policy-making.

This is an open access article under the terms of the Creative Commons Attribution License, which permits use, distribution and reproduction in any medium, provided the original work is properly cited.

© 2025 The Author(s). *Engineering Reports* published by John Wiley & Sons Ltd.

1 | Introduction

Malaria, caused by *Plasmodium* parasites and transmitted by female *Anopheles* mosquitoes, remains a major public health challenge in tropical and subtropical regions. Endemic in over 80 countries, primarily in sub-Saharan Africa, Southeast Asia, and parts of South America, it caused an estimated 249 million cases and 619,000 deaths in 2022 [1]. More than 90% of malaria-related deaths occur in sub-Saharan Africa, disproportionately affecting children under five and impoverished communities [1–3]. Incidence rates have declined over recent years due to interventions such as insecticide-treated nets (ITNs), indoor residual spraying (IRS), and artemisinin-based combination therapies. However, rising resistance in mosquitoes to insecticides and in parasites to antimalarial drugs has made malaria harder to control, especially in high-transmission areas [4]. These challenges have shifted research towards new control strategies, including malaria vaccines, gene-editing technologies, and eco-friendly larvicidal approaches [3, 4]. The disease also imposes an economic burden, with losses of up to 1.3% of GDP in severely affected African nations, and it particularly endangers pregnant women and young children [4].

Progress has stalled since 2017, especially in high-burden countries like Nigeria, the Democratic Republic of Congo, and Uganda. Contributing factors include limited healthcare access, humanitarian crises, and funding gaps. To address these, initiatives such as the "High Burden to High Impact" approach are used to accelerate malaria elimination [2].

Although the most harmful diseases in the world [5–12], malaria is curable with prompt and accurate diagnosis and treatment [13]. The primary culprits—*Plasmodium falciparum* and *Plasmodium vivax*—invade red blood cells and are spread through bites from infected female *Anopheles* mosquitoes [14].

Among promising interventions, larval source management (LSM), including larviciding, habitat modification, and biological control, targets mosquito immatures. Plant-based larvicides offer an eco-friendly alternative to synthetic chemicals, with several medicinal extracts showing potent larvicidal properties [15, 16]. Reducing larval habitats limits mosquito population growth and transmission. Killeen et al. [17] modeled this by incorporating reduced human bite rates. The World Health Organization (WHO) recommends larviciding as a supplementary measure, particularly in urban or dry-season settings where breeding sites are few and fixed [18, 19]. This study explores the larvicidal potential of medicinal plant extracts, modeled using fractal fractional derivatives. Compartmental modeling has been widely used to understand different health problems and can be extended to malaria transmission dynamics. It supports the evaluation of interventions and the prediction of outbreak trends based on biological, social, and ecological factors [20–24]. These models, when fitted to real data, help estimate key parameters, guiding the design of effective control strategies [25–40]. For instance, [41] demonstrated how combining interventions can enable elimination, while [42] introduced an agent-based model to predict malaria peak seasons. The use of fractional orders and their combinations for solving physical problems with real data fitting, particularly using the Atangana–Baleanu (ABC) operator, has been proposed [43, 44].

Recently, the combination of fractal and fractional derivatives led to the creation of a new operator referred to as a fractal-fractional (FF) operator [45–52]. The FF order models outperform integer-order models, with [46] proving that these operators are more suitable for fitting real-world problems. Additionally, the findings [45, 46] suggest that varying both the fractal and fractional orders yields interesting results. Numerical analysis of this new operator is discussed [47–52]. The authors in [53] introduce an operator called fractal-fractional derivatives, which bridges fractal calculus and fractional calculus. Atangana [53] also investigates fractal-fractional integrals. These derivatives integrate the Mittag-Leffler law, exponential law, and power law with fractal derivatives, comprising two components: fractional order and fractal dimension. The idea of FF has been used to study tuberculosis and diabetes mellitus with co-infection of the COVID-19 virus model [54, 55]. Given the high accuracy of these operators in simulating fractal-fractional systems, many researchers have focused on fractal-fractional models, for example, in malaria problems [56].

This paper introduces an innovative model of malaria dynamics using integer and fractal fractional order derivatives. The aim is to raise social and academic awareness about using biological insecticides (plant leaf extracts) in killing mosquito larvae and controlling malaria. The fractal–fractional order larvicidal model bridges mathematical modeling with practical public health applications. By optimizing larvicide application, reducing environmental impact, and supporting sustainable policies, the model offers a comprehensive approach to mosquito population control. This directly contributes to reducing malaria transmission, improving environmental health, and safeguarding public health in malaria-endemic regions. The model promotes eco-friendly larvicide applications, sustainable bio-larvicides, and targeting high-risk breeding hotspots for resource-efficient interventions. It supports data-driven policymaking to minimize environmental impact and insecticide resistance, ensuring long-term vector control effectiveness. Additionally, the model helps lower malaria transmission rates, improve health outcomes, reduce healthcare costs, and promote public awareness and community participation in environmentally conscious control measures.

To the best of our knowledge, this paper offers an innovative perspective on health informatics by integrating compartmental modeling (CM) and fractal-fractional calculus to control malaria using larvicidal plant extracts. The proposed CM framework bridges traditional disease control methods with modern digital technologies, including the Internet of Things (IoT) and Artificial Intelligence (AI).

1.1 | Summary of Contributions

This study explores the larvicidal potential of medicinal plant extracts and uses fractal-fractional modeling to evaluate their effectiveness in reducing Anopheles mosquito populations and ultimately curbing malaria transmission.

The main contributions of this paper are:

- formulating an integrated CM for managing mosquito breeding and malaria spread among human populations



FIGURE 1 | (a–d) *Petiveria alliacea* plant (a), grounded *Petiveria alliacea* plant (b), *Hyptis suavolens* plant (c), grounded *Hyptis suavolens* plant (d).

using larvicidal plant extracts (*Petiveria alliacea* and *Hyptis suaveolens*), implemented through fractal-fractional models (FFM) to capture memory effects and reinfection dynamics, fractal and non-locality properties of mosquitoes;

- adaptation of the memory property of the model to characterize susceptibility and reinfection of hosts. This study also models the non-local property of FFM to discuss wider coverage of host interactions with the disease vector and environment. The model uses the fractal property of FFM to capture and evaluate the heterogeneous breeding and survival domains of the disease-bearing mosquitoes—the adult female Anopheles;
- formulating and evaluating the basic reproduction number of *Anopheles* mosquitoes based on stability and control analysis principles of the Hyers-Ulam stability method, to determine the control efficacy of the proposed FFM-based model;
- modeling, design, and simulation of the combined effects of treating mosquito nets with plant-based extracts that contain naturally occurring larvicides;
- design and modeling of a smart larvicidal-treated mosquito net framework integrated with IoT-enabled data collection, processing, and cloud-based CM using AWS EC2 instances. Our approach demonstrates scalable, AI-ready solutions for epidemic control and policy-making.

The remaining sections of the article are organized as follows: Section 2 provides model formulation, Section 3 introduces the fractal-fractional-order generalization of the proposed model, Section 4 presents the numerical algorithm for the fractal fractional derivative, while Section 5 includes graphical analyses and discussions. Finally, Section 6 concludes the study and highlights future directions for the model.

2 | Problem Model Formulation

We present the compartmental model of larvicidal plant extracts for controlling malaria using Caputo–Fabrizio fractal-fractional derivatives and focusing on two populations: humans and mosquitoes. A novel numerical method is employed to solve these generalized operators. Lagrangian piecewise interpolation was used to provide solutions with both fractal and fractional parameters. Additionally, we propose a control strategy involving *Petiveria alliacea* and *Hyptis suavolens* leaf extracts, leveraging their larvicidal properties. In this context, *Hyptis suavolens* and *Petiveria alliacea* leaf extracts are explored to reduce mosquito populations (see Figure 1a–d).

TABLE 1 | Description of the compartments.

Compartment	Description
S_h	Susceptible human at time t.
E_h	Exposed human at time t.
I_h	Infected human at time t.
T_h	Treated human at time t.
R_h	Recovered human at time t.
S_m	Susceptible mosquitoes at time t.
E_m	Exposed mosquitoes at time t.
I_m	Infected mosquitoes at time t.

This study investigates a compartmental model involving a set of human beings mixing up in a community and another set of mosquito populations also mixing up in the community. The set human population includes the susceptible (S_h), exposed (E_h), infected (I_h), treated (T_h) and recovered (R_h) groups of persons. The set of mosquito populations includes the susceptible (S_m), exposed (E_m) and infected (I_m) mosquito compartments. Based on these compartments, the study sets out a compartmental model of five human parameters denoted as "*SEITR*" for the host population and "*SEI*" for the vector population, analogous to established frameworks [57–61], (see Table 1). Our model incorporates biting rate (δ) and transmission rates β_h for humans (i.e., host) and β_m for mosquitoes (i.e., vector), capturing the complex dynamics of malaria transmission. We consider both human and mosquito populations, with total populations denoted as $N_h(t)$ and $N_m(t)$, respectively. For the host population, the *SEITR*

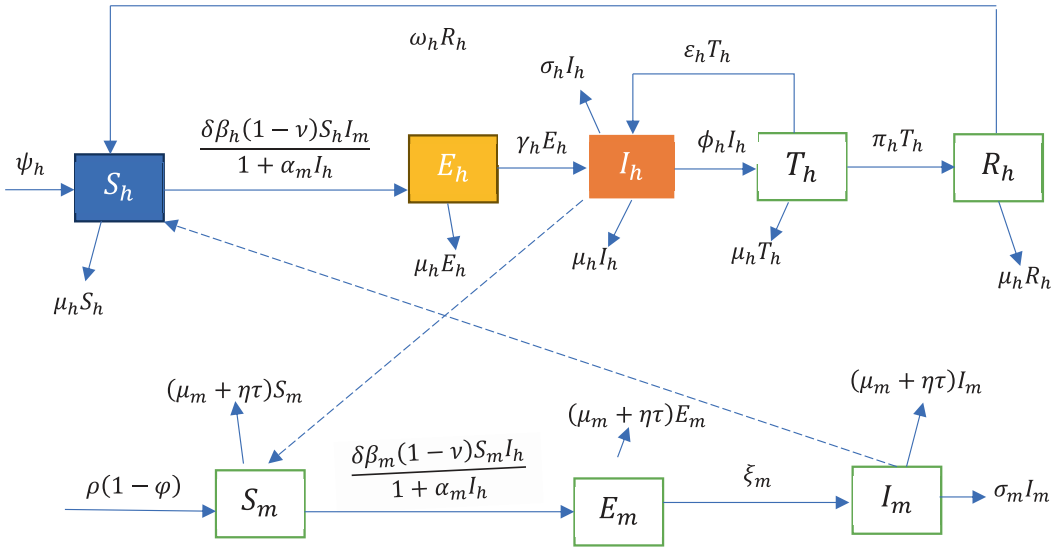


FIGURE 2 | Compartmental flow diagram of how malaria spreads within a given population. It incorporates the use of larvicidal plant extracts to mitigate the contraction and spread of the disease vector within a community by considering two populations: The human population (upper) and the mosquito (lower) diagram).

model describes the total human population dynamics at time t given by

$$N_h(t) = S_h(t) + E_h(t) + I_h(t) + T_h(t) + R_h(t)$$

While the *SEI* model captures the total mosquito population dynamics at time t, given by

$$N_m(t) = S_m(t) + E_m(t) + I_m(t)$$

The following assumptions are made to formulate the equations of the model:

- The prevention strategies contribute to the death rate of the mosquitoes that bite and transmit malaria to humans [62–64].
- Larvicides reduce the population of the adult mosquitoes, thereby reducing the transmission rate [65, 66].
- The infected human population recovers after treatment with temporary immunity.
- Mosquitoes do not die from the infection [67, 68].
- All hosts and vectors are susceptible to malaria infection [69].

The transition diagram for the proposed model is presented in Figure 2. Tables 1 and 2 show the variables and parameters used in the compartmental model and their interpretations. The systems of the following equations are obtained from the transition diagram shown in Figure 2:

Consequently, a system of non-linear ordinary differential equations is given below based on the descriptions:

$$\left.\begin{aligned}
\frac{dS_h(t)}{dt} &= \psi_h + \omega_h R_h(t) - \frac{\delta\beta_h(1-\nu)S_h(t)I_m(t)}{1+\alpha_h I_m(t)} - \mu_h S_h(t)\\
\frac{dE_h(t)}{dt} &= \frac{\delta\beta_h(1-\nu)S_h(t)I_m(t)}{1+\alpha_h I_m(t)} - \left(\mu_h+\gamma_h\right)E_h(t)\\
\frac{dI_h(t)}{dt} &= \gamma_h E_h(t) + \varepsilon_h T_h(t) - \left(\mu_h+\phi_h+\sigma_h\right)I_h(t)\\
\frac{dT_h(t)}{dt} &= \phi_h I_h(t) - \left(\mu_h+\varepsilon_h+\pi_h\right)T_h(t)\\
\frac{dR_h(t)}{dt} &= \pi_h T_h(t) - \left(\mu_h+\omega_h\right)R_h(t)\\
\frac{dS_m(t)}{dt} &= \rho(1-\varphi) - \left(\mu_m+\eta\tau\right)S_m(t) - \frac{\delta\beta_m(1-\nu)S_m(t)I_h(t)}{1+\alpha_m I_h(t)}\\
\frac{dE_m(t)}{dt} &= \frac{\delta\beta_m(1-\nu)S_m(t)I_h(t)}{1+\alpha_m I_h(t)} - \left(\mu_m+\xi_m+\eta\tau\right)E_m(t)\\
\frac{dI_m(t)}{dt} &= \xi_m E_m(t) - \left(\mu_m+\eta\tau+\sigma_m\right)I_m(t)
\end{aligned}\right\} \quad (1)$$

with initial conditions

$$\begin{aligned}
S_h(0) = S_{h0}, E_h(0) = E_{h0}, I_h(0) = I_{h0}, T_h(0) = T_{h0}, R_h(0)\\
= R_{h0}, S_m(0) = S_{m0}, E_m(0) = E_{m0}, I_m(0) = I_{m0}
\end{aligned} \quad (2)$$

We used a saturated incidence of the form $\frac{\delta\beta_h(1-\nu)S_h(t)I_m(t)}{1+\alpha_h I_m(t)}$, where $\delta\beta_h(1-\nu)S_h(t)I_m(t)$ is a bilinear incidence that shows the rate at which susceptible humans are infected by infectious mosquitoes and $\frac{1}{1+\alpha_h I_m(t)}$ represents a saturated feature that inhibits the force of infection from infectious mosquitoes to susceptible humans. In other words, it produces antibodies at $\alpha_h \in [0,1]$ in response to the presence of antigens (in the form of parasites) produced by infectious Anopheles mosquitoes. Similarly, we have a saturated force of infection of the form: $\frac{\delta\beta_m(1-\nu)S_m(t)I_h(t)}{1+\alpha_m I_h(t)}$ where $\delta\beta_m(1-\nu)S_m(t)I_h(t)$ is the rate at which the susceptible mosquitoes are infected by the infectious humans, while $\frac{1}{1+\alpha_m I_h(t)}$ denotes a saturated feature that inhibits the force of infection from infectious humans to susceptible mosquitoes. Subsequently, mosquitoes have DNA like humans [74]; they also develop antibodies against the malaria parasites [75]. Thus, $\alpha_m \in [0,1]$ is the rate at which antibodies are produced against the antigens contacted by infected humans.

TABLE 2 | Parameter descriptions.

Parameter	Description	Value	Source
ψ_h	Human recruitment rate	0.000215	[61]
β_h	Infection rate from mosquitoes to humans	0.1	[61]
β_m	Infection rate from humans to mosquitoes	0.09	[61]
μ_h	The natural death rate of humans	0.000548	[61]
υ	Reduction of infection rate due to the use of treated mosquito nets	0.53	[70]
γ_h	Progression rate of exposed human to infected human	0.05882	[61]
ε_h	Treatment failure rate of the infected $I_h(t)$ due to the ineffectiveness of antimalarial drugs or inappropriate dosage	0.0003	Fitted
ϕ_h	Progression rate of infected human to treated human	0.3	[38, 71]
σ_h	Disease-induced death rate of humans due to malaria infection	0.001	[61]
σ_m	Disease-induced death rate of mosquitoes due to malaria infection	0.1	Fitted
π_h	Progression rate of treated human to recovered human (expected recovery rate of $T_h(t)$)	0.05	[61]
ω_h	Waning immunity rate of $R_h(t)$	0.0001370	[61]
μ_m	The natural death rate of mosquitoes	0.067	[61]
ρ	Mosquito recruitment birth rate	0.7	Fitted
φ	Larvicidal activity that reduces the mosquito population	0.85	Estimated
$\eta\tau$	Prevention effort that contributes to the vector death rate	0.0025	[72]
α_m	The parameter that measures the inhibitory effects of transmission from humans to mosquitoes	0.04	[73]
α_h	The parameter that measures the inhibitory effects of transmission from mosquitoes to humans	0.06	[73]
δ	The biting rate of the mosquitoes	0.12	[61]
ξ_m	The progression rate of exposed mosquitoes to infectious mosquitoes	0.56	[61]
η	Proportion of prevention rate, $0 \leq \eta \leq 1$	0.05	[72]

2.1 | Analysis of the Model

2.1.1 | Invariant Region

The invariant region is used to determine where the model's solution is bound. We therefore provide the following results, which guarantee that the malaria model governed by system (1) is epidemiologically and mathematically well-posed in the feasible region Γ given by:

$$\Gamma = \Gamma_h \times \Gamma_m \subseteq \mathbb{R}_+^5 \times \mathbb{R}_+^3 \tag{3}$$

where

$$\Gamma_h = \left\{ \left(S_h, E_h, I_h, T_h, R_h\right) \in \mathbb{R}_+^5 : 0 \leq S_h + E_h + I_h + T_h + R_h \leq \frac{\psi_h}{\mu_h} \right\} \tag{4}$$

and

$$\Gamma_m = \left\{ \left(S_m, E_m, I_m\right) \in \mathbb{R}_+^3 : 0 \leq S_m + E_m + I_m \leq \frac{\rho(1-\varphi)}{\mu_m} \right\} \tag{5}$$

Is a positive invariant. Thus, all solutions for the human population are confined to the feasible region Γ_h and all solutions of the mosquito population are confined to Γ_m. As a result, the system's invariant region for the formulated model system (1) exists and is given by:

$$\Gamma = \left\{ \left(S_h, E_h, I_h, T_h, R_h, S_m, E_m, I_m\right) \in \mathbb{R}_+^8 : N_h \leq \frac{\psi_h}{\mu_h}, N_m \leq \frac{\rho(1-\varphi)}{\mu_m} \right\} \tag{6}$$

Is a positive invariant set, and all the solutions of system (1) are bounded in Γ within the region. It remains to show that the solutions of system (1) are non-negative in Γ for all $t > 0$ since the model represents human and mosquito populations.

2.1.2 | Positivity of Solution

Theorem 1. *There exists a domain Γ in which the solution set of a system (1) is given by $S_h, E_h, I_h, T_h, R_h, S_m, E_m$ and I_m with non-negative initial conditions $S_h(0), E_h(0), I_h(0), T_h(0) = R_h(0), S_m(0), E_m(0)$, and $I_m(0)$ remains non-negative for all time $t \geq 0$.*

Proof. By taking the first equation of system (1), we have

$$\frac{dS_h(t)}{dt} = \psi_h + \omega_h R_h(t) - \frac{\delta\beta_h(1-\nu)S_h(t)I_m(t)}{1+\alpha_h I_m(t)} - \mu_h S_h(t) \tag{7}$$

$$\frac{dS_h(t)}{dt} \geq -\left(\frac{\delta\beta_h(1-\nu)I_m(t)}{1+\alpha_h I_m(t)} + \mu_h\right) S_h(t) \tag{8}$$

Integrating Equation (8) for time and using the technique of variable separation with the initial condition, we obtain

$$S_h(t) \geq S_h(0) \exp\left\{-\left(\mu_h t + \int_0^t \left(\frac{\delta\beta_h(1-\nu)I_m(\theta)}{1+\alpha_h I_m(\theta)}\right)\right)d\theta\right\} \geq 0 \tag{9}$$

This implies that $S_h(t) > 0$ for all $t > 0$. □

Similarly, it can be proved that the other state variables $E_h(t), I_h(t), T_h(t), R_h(t), S_m(t), E_m(t)$ and $I_m(t)$ are solved using the remaining sub-equations of the system (1) for all time $t > 0$ by the same procedure. Thus, we obtain

$$\left.\begin{array}{l} E_h(t) \geq E_h(0)\exp\left\{-\left(\mu_h+\gamma_h\right)t\right\} \geq 0, \quad I_h(t) \geq I_h(0)\exp\left\{-\left(\mu_h+\phi_h+\sigma_h\right)t\right\} \geq 0 \\ T_h(t) \geq T_h(0)\exp\left\{-\left(\mu_h+\varepsilon_h+\pi_h\right)t\right\} \geq 0, \quad R_h(t) \geq R_h(0)\exp\left\{-\left(\mu_h+\omega_h\right)t\right\} \geq 0 \\ S_m(t) \geq S_m(0)\exp\left\{-\left(\mu_m+\eta\tau+\int_0^t\left(\frac{\delta\beta_m(1-\nu)I_h(\theta)}{1+\alpha_m I_h(\theta)}\right)\right)d\theta\right\} \geq 0 \\ E_m(t) \geq E_m(0)\exp\left\{-\left(\mu_m+\xi_m+\eta\tau\right)t\right\} \geq 0, \quad I_m(t) \geq I_m(0)exp\left\{-\left(\mu_m+\eta\tau+\sigma_m\right)t\right\} \geq 0 \end{array}\right\} \tag{10}$$

This completes the proof, and as a result, the malaria transmission model with larvicidal activity stated in System (1) is both epidemiologically and mathematically well-posed in Γ.

2.2 | Existence and Stability of Equilibrium Points

Equilibrium points or steady-state solutions are the points at which the proposed model system (1) is equal to zero. As long as the recruitment term ψ_h and $\rho(1-\varphi)$ are not zero, there will be no trivial equilibrium points, which implies that $\left(S_h^*, E_h^*, I_h^*, T_h^*, R_h^*, S_m^*, E_m^*, I_m^*\right) \neq (0,0,0,0,0,0,0,0)$ and the populations will not be extinct.

2.2.1 | Existence of Disease-Free Equilibrium Point (DFEP)

To obtain the steady-state solution or the disease-free equilibrium point of the model system (1), we equate the left-hand side to zero, and this implies there is no malaria infection in the population. Thus, we obtain

$$E_0 = \left(\frac{\psi_h}{\mu_h}, 0, 0, 0, 0, \frac{\rho(1-\varphi)}{\mu_m}, 0, 0\right) \tag{11}$$

2.2.2 | Existence of Endemic Equilibrium Point (EEP)

The potential existence of an endemic equilibrium point, represented by the notation E^*, will be investigated below, and denoted as

$$E^* = \left(S_h^*(t), E_h^*(t), I_h^*(t), T_h^*(t), R_h^*(t), S_m^*(t), E_m^*(t), I_m^*(t)\right)$$

Therefore, we compute the endemic equilibrium of system (1) as follows:

$$\left.\begin{array}{ll} S_h^* = \frac{\left(\psi_h+\omega_h R_h^*\right)\left(1+\alpha_h I_m^*\right)}{\delta\beta_h(1-\nu)I_m^*+\mu_h\left(1+\alpha_h I_m^*\right)}, & E_h^* = \frac{\delta\beta_h(1-\nu)S_h^* I_m^*}{\left(1+\alpha_h I_m^*\right)\left(\mu_h+\gamma_h\right)} \\ I_h^* = \frac{\gamma_h E_h^*+\varepsilon_h T_h^*}{\left(\mu_h+\phi_h+\sigma_h\right)}, & T_h^* = \frac{\phi_h I_h^*}{\left(\mu_h+\varepsilon_h+\pi_h\right)}, \quad R_h^* = \frac{\pi_h T_h^*}{\left(\mu_h+\omega_h\right)} \\ S_m^* = \frac{\rho(1-\varphi)\left(1+\alpha_m I_h^*\right)}{\left(\mu_m+\eta\tau\right)\left(1+\alpha_m I_h^*\right)+\delta\beta_m(1-\nu)I_h^*} & \\ E_m^* = \frac{\delta\beta_m(1-\nu)S_m^* I_h^*}{\left(1+\alpha_m I_h^*\right)\left(\mu_m+\xi_m+\eta\tau\right)}, & I_m^* = \frac{\xi_m E_m^*}{\left(\mu_m+\eta\tau+\sigma_m\right)} \end{array}\right\} \tag{12}$$

2.3 | Basic Reproduction Number (R_0)

The basic reproduction number is the average number of secondary infections produced by a single infected individual in a completely susceptible population over a given period. We therefore use the next-generation matrix method to obtain the reproduction number, R_0. To get at R_0 at E_0, we rewrite model system (1) beginning with newly infective classes of human and mosquito populations as

$$\left.\begin{array}{l} \frac{dE_h(t)}{dt} = \frac{\delta\beta_h(1-\nu)S_h(t)I_m(t)}{1+\alpha_h I_m(t)} - \left(\mu_h+\gamma_h\right)E_h(t) \\ \frac{dI_h(t)}{dt} = \gamma_h E_h(t) + \varepsilon_h T_h(t) - \left(\mu_h+\phi_h+\sigma_h\right)I_h(t) \\ \frac{dE_m(t)}{dt} = \frac{\delta\beta_m(1-\nu)S_m(t)I_h(t)}{1+\alpha_m I_h(t)} - \left(\mu_m+\xi_m+\eta\tau\right)E_m(t) \\ \frac{dI_m(t)}{dt} = \xi_m E_m(t) - \left(\mu_m+\eta\tau+\sigma_m\right)I_m(t) \end{array}\right\} \tag{13}$$

Let $\mathcal{G} = \left(E_h(t), I_h(t), E_m(t), I_m(t)\right)$ then $\frac{d\mathcal{G}}{dt} = F(\mathcal{G}) - V(\mathcal{G})$, where

$$F = \begin{bmatrix} \frac{\delta\beta_h(1-\nu)S_h I_m}{1+\alpha_h I_m} \\ 0 \\ \frac{\delta\beta_m(1-\nu)S_m I_h}{1+\alpha_m I_h} \\ 0 \end{bmatrix} \quad \text{and} \quad V = \begin{bmatrix} \left(\mu_h+\gamma_h\right)E_h \\ -\gamma_h E_h - \varepsilon_h T_h + \left(\mu_h+\phi_h+\sigma_h\right)I_h \\ \left(\mu_m+\xi_m+\eta\tau\right)E_m \\ -\xi_m E_m + \left(\mu_m+\eta\tau+\sigma_m\right)I_m \end{bmatrix} \tag{14}$$

The Jacobian matrices of F and V at the disease-free equilibrium points give F and V, respectively, as

$$F = \begin{bmatrix} 0 & 0 & 0 & \frac{\delta\beta_h\psi_h(1-\upsilon)}{\mu_{ha}} \\ 0 & 0 & 0 & 0 \\ 0 & \frac{\delta\beta_m\rho(1-\upsilon)(1-\varphi)}{\mu_m} & 0 & 0 \\ 0 & 0 & 0 & 0 \end{bmatrix}$$

and

$$V = \begin{bmatrix} A_{11} & 0 & 0 & 0 \\ -\gamma_h & A_{22} & 0 & 0 \\ 0 & 0 & A_{33} & 0 \\ 0 & 0 & -\xi_m & A_{44} \end{bmatrix}$$

where $A_{11} = \mu_h + \gamma_h, A_{22} = \mu_h + \phi_h + \sigma_h, A_{33} = \mu_m + \xi_m + \eta\tau$, and $A_{44} = \mu_m + \eta\tau + \sigma_m$.

$$V^{-1} = \begin{bmatrix} P_{11} & 0 & 0 & 0 \\ P_{21} & P_{22} & 0 & 0 \\ 0 & 0 & P_{33} & 0 \\ 0 & 0 & P_{43} & P_{44} \end{bmatrix} \tag{15}$$

where $P_{11} = \frac{1}{(\mu_h+\gamma_h)}, P_{21} = \frac{\gamma_h}{(\mu_h+\gamma_h)(\mu_h+\phi_h+\sigma_h)}, P_{22} = \frac{1}{(\mu_h+\phi_h+\sigma_h)}, P_{33} = \frac{1}{(\mu_m+\xi_m+\eta\tau)}, P_{43} = \frac{\xi_m}{(\mu_m+\xi_m+\eta\tau)(\mu_m+\eta\tau+\sigma_m)}, P_{44} = \frac{1}{(\mu_m+\eta\tau+\sigma_m)}$.

$$FV^{-1} = \begin{bmatrix} 0 & 0 & K_{13} & K_{14} \\ 0 & 0 & 0 & 0 \\ K_{31} & K_{32} & 0 & 0 \\ 0 & 0 & 0 & 0 \end{bmatrix} \tag{16}$$

where $K_{13} = \frac{\delta\beta_h\psi_h\xi_m(1-\nu)}{\mu_h(\mu_m+\xi_m+\eta\tau)(\mu_m+\eta\tau+\sigma_m)}, K_{14} = \frac{\delta\beta_h\psi_h(1-\nu)}{\mu_h(\mu_m+\eta\tau+\sigma_m)}, K_{31} = \frac{\delta\beta_m\rho(1-\nu)(1-\varphi)}{\mu_m(\mu_h+\gamma_h)(\mu_h+\phi_h+\sigma_h)}, K_{32} = \frac{\delta\beta_m\rho(1-\nu)(1-\varphi)}{\mu_m(\mu_h+\phi_h+\sigma_h)}$.

$$FV^{-1} = \begin{bmatrix} 0 & \frac{\delta\beta_h\psi_h\xi_m(1-\nu)}{\mu_h(\mu_m+\xi_m+\eta\tau)(\mu_m+\eta\tau+\sigma_m)} \\ \frac{\delta\beta_m\rho\gamma_h(1-\nu)(1-\varphi)}{\mu_m(\mu_h+\gamma_h)(\mu_h+\phi_h+\sigma_h)} & 0 \end{bmatrix} \tag{17}$$

The fundamental basic reproduction number, $R_0 = \Lambda(FV^{-1})$, is the spectral radius of the product derived from the new infection matrix and the inverse of the transmission or transfer matrix. The basic reproduction number R_0 can be obtained from the trace and determinant of the matrix by letting $FV^{-1} = G$. Therefore

$$R_0 = \Lambda(\mathrm{G}) = \frac{1}{2}\left(trace\,(G) + \sqrt{trace\,(G)^2 - 4\det(G)}\right) \tag{18}$$

Observe that $trace\,(G) = 0$, so that we have

$$R_0 = \frac{1}{2}\sqrt{\frac{4\left(\delta^2\beta_m\beta_h\psi_h\gamma_h\xi_m\rho(1-\nu)^2(1-\varphi)\right)}{\mu_h\mu_m(\mu_h+\gamma_h)(\mu_h+\phi_h+\sigma_h)(\mu_m+\xi_m+\eta\tau)(\mu_m+\eta\tau+\sigma_m)}}$$

$$R_0 = \sqrt{\frac{\left(\delta^2\beta_m\beta_h\psi_h\gamma_h\xi_m\rho(1-\nu)^2(1-\varphi)\right)}{\mu_h\mu_m(\mu_h+\gamma_h)(\mu_h+\phi_h+\sigma_h)(\mu_m+\xi_m+\eta\tau)(\mu_m+\eta\tau+\sigma_m)}} \tag{19}$$

From Equation (19), if we have that $\frac{\gamma_h}{(\mu_h+\gamma_h)}$ represents the probability that a human will survive the exposed state to become infectious; $\frac{1}{(\mu_h+\phi_h+\sigma_h)}$ represents the average duration of the infectious period of the human; $\frac{\xi_m}{(\mu_m+\xi_m+\eta\tau)}$ denotes the probability that a mosquito will survive the exposed state to become infectious and $\frac{1}{(\mu_m+\eta\tau+\sigma_m)}$ denotes a state to become infectious; $\frac{1}{(\mu_h+\phi_h+\sigma_h)}$ is the average duration of the infectious period of the mosquito. Then, the basic reproduction number R_0 can be rewritten as

$$R_0 = \sqrt{R_{0h}R_{0m}} \tag{20}$$

where

$$R_{0h} = \frac{\delta\beta_m\gamma_h\rho(1-\nu)(1-\varphi)}{\mu_m(\mu_h+\gamma_h)(\mu_h+\phi_h+\sigma_h)} \text{ and } R_{0m} = \frac{\delta\beta_h\psi_h\xi_m(1-\nu)}{\mu_h(\mu_m+\xi_m+\eta\tau)(\mu_m+\eta\tau+\sigma_m)}$$

We denote that R_{0h} is the number of humans that one infectious mosquito infects over its expected infection period in a completely susceptible human population. Similarly, R_{0m} describes the number of mosquitoes infected by one infectious human during the period of infectiousness in a completely susceptible mosquito population.

Theorem 2. *The larvicidal control of malaria-free equilibrium of (1) given by (11) is locally asymptotically stable if* $R_{0h} \leq 1$ *and* $R_m \leq 1\,(or\ R_0 \leq 1)$ *and unstable if* $R_{0h} > 1$ *and* $R_{0m} > 1\,(or\ R_0 > 1)$.

The epidemiological suggestion is that malaria infection can be eradicated from the population only when the basic reproduction number is less than unity (i.e., $R_0 \leq 1$). This means that $R_0 < 1$ must be less than unity $(R_{0h} \leq 1)$ and $(R_{0m} \leq 1)$ less than unity $(R_0 \leq 1)$, if the initial concentration of the model compartments is in the basin of attraction of Γ. The local stability of the larvicidal control of the malaria-free equilibrium point is computed with the Jacobian matrix of (1) at E_0 and thus:

$$J_{(E_0)} = \begin{bmatrix} J_{11} & 0 & 0 & 0 & J_{15} & 0 & 0 & J_{18} \\ 0 & J_{22} & 0 & 0 & 0 & 0 & 0 & J_{28} \\ 0 & J_{32} & J_{33} & J_{34} & 0 & 0 & 0 & 0 \\ 0 & 0 & J_{43} & J_{44} & 0 & 0 & 0 & 0 \\ 0 & 0 & 0 & J_{54} & J_{55} & 0 & 0 & 0 \\ 0 & 0 & J_{63} & 0 & 0 & J_{66} & 0 & 0 \\ 0 & 0 & J_{73} & 0 & 0 & 0 & J_{77} & 0 \\ 0 & 0 & 0 & 0 & 0 & 0 & J_{87} & J_{88} \end{bmatrix} \tag{21}$$

where $J_{11} = -\mu_h, J_{15} = \omega_h, J_{18} = -\frac{\delta\beta_h(1-\nu)\psi_h}{\mu_h}, J_{22} = -(\mu_h+\gamma_h), J_{28} = \frac{\delta\beta_h(1-\nu)\psi_h}{\mu_h}, J_{32} = \gamma_h,\ J_{33} = -(\mu_h+\phi_h+\sigma_h), J_{34} = \varepsilon_h, J_{43} = \phi_h, J_{44} = -(\mu_h+\varepsilon_h+\pi_h), J_{54} = \pi_h, J_{55} = -(\mu_h+\omega_h), J_{63} = -\frac{\delta\beta_m(1-\nu)\rho(1-\varphi)}{\mu_m}, J_{66} = -(\mu_m+\eta\tau), J_{73} = \frac{\delta\beta_m(1-\nu)\rho(1-\varphi)}{\mu_m}, J_{77} = -(\mu_m+\xi_m+\eta\tau), J_{87} = \xi_m, J_{88} = -(\mu_m+\eta\tau+\sigma_m)$. If we observe critically the form of the Jacobian matrix, we immediately see that: $J_{11} = -\mu_h,\ J_{55} = -(\mu_h+\omega_h)$ and $J_{66} = -(\mu_m+\eta\tau)$ are eigenvalues. The remaining eigenvalues are those of the 5×5 submatrix.

$$J(E_0^*) = \begin{bmatrix} J_{22} & 0 & 0 & 0 & J_{28} \\ J_{32} & J_{33} & J_{34} & 0 & 0 \\ 0 & J_{43} & J_{44} & 0 & 0 \\ 0 & J_{73} & 0 & J_{77} & 0 \\ 0 & 0 & 0 & J_{87} & J_{88} \end{bmatrix}$$

The characteristic equation of $J(E_0^*)$ of (1) at E_0 is of the form $\left|J(E_0^*) - \lambda I\right| = 0$ can be given as

$$\begin{aligned} &\lambda^5 + [A + C + D + G + H]\lambda^4 + [AC + AD + AG + AH + CD + CG \\ &\quad + CH + DG + DH + GH - \phi_h\varepsilon_h]\lambda^3 \\ &\quad + [ACD + ACG + ACH + ADG + ADH + AGH + CDH \\ &\quad + CDG + CGH + DGH - A\phi_h\varepsilon_h - G\phi_h\varepsilon_h - H\phi_h\varepsilon_h]\lambda^2 \\ &\quad + [ACDH + ACDG + ADGH + CDGH + (1 - R_0) - AH\phi_h\varepsilon_h - GH\phi_h\varepsilon_h]\lambda \\ &\quad + [(1 - R_0) - AGH\phi_h\varepsilon_h] = 0 \end{aligned} \tag{22}$$

with $-A = J_{22}, B = J_{28}, -C = J_{33}, -D = J_{44}, E = J_{73}, -G = J_{77}, -H = J_{88}$.

We can rewrite system (22) into

$$\lambda^5 + d_1\lambda^4 + d_2\lambda^3 + d_3\lambda^2 + d_4\lambda + d_5 = 0 \tag{23}$$

where

$$\left.\begin{aligned} d_1 &= A + C + D + G + H \\ d_2 &= AC + AD + AG + AH + CD + CG + CH + DG + DH \\ &\quad + GH - \phi_h\varepsilon_h \\ d_3 &= CD + ACG + ACH + ADG + ADH + AGH + CDH + CDG \\ &\quad + CGH + DGH - A\phi_h\varepsilon_h - G\phi_h\varepsilon_h - H\phi_h\varepsilon_h \\ d_4 &= ACDH + ACDG + ADGH + CDGH + \left(1 - R_0\right) \\ &\quad - AH\phi_h\varepsilon_h - GH\phi_h\varepsilon_h \\ d_5 &= \left(1 - R_0\right) - AGH\phi_h\varepsilon_h \end{aligned}\right\} \tag{24}$$

By the Routh-Hurwitz criterion, it follows that all roots of the characteristic Equation (23) have a negative real part if and only if

$$\begin{aligned} d_1d_2d_3 > d_3^2 + d_1^2d_4 \text{ and } \left(d_1d_4 - d_5\right)\left(d_1d_2d_3 - d_3^2 - d_1^2d_4\right) \\ > d_5\left(d_1d_2 - d_3\right)^2 + d_1d_5^2 \end{aligned} \tag{25}$$

Therefore, from (24) we have that all roots of (23) will have a negative real part if and only if it satisfies (25) and $R_0 \leq 1$.

3 | Fractal Fractional-Order Generalization of the Model

3.1 | Preliminaries

We will describe a few significant concepts in fractal-fractional calculus. Additional information on this innovative use of calculus can be found in [76].

Definition 1. Atangana [77]. The fractal fractional derivative of $f(t)$ with order $\hbar - \mathscr{E}$ in the Riemann-Liouville sense is defined as follows:

$${}_0^{FF-RL}D_{0,t}^{\mathscr{E},\hbar}\{f(t)\} = \frac{1}{\Omega(g-\mathscr{E})}\frac{d}{dt^\hbar}\int_0^t (t-s)^{g-\mathscr{E}-1}f(s)ds \tag{26}$$

where $g - 1 = \mathscr{E}, \hbar \leq g \in \mathbb{N}$ *and* $\frac{df(s)}{ds^\hbar} = Lim_{t\to s}\frac{f(t)-f(s)}{t^\hbar - s^\hbar}$.

Definition 2. References [78–80]. The fractal-fractional integral of $f(t)$ with fractional order $\mathscr{E}$ and an exponentially decaying kernel, assuming that $f(t)$ is fractally integrable and continuous over some open interval (x, y) with fractal order $\hbar$, is defined as follows:

$${}_0^{FF}D_{0,t}^{\mathscr{E},\hbar}\{f(t)\} = \frac{\hbar(1-\mathscr{E})t^{\hbar-1}f(t)}{\mathcal{P}(\mathscr{E})} + \frac{\mathscr{E}\hbar}{\mathcal{P}(\mathscr{E})}\int_0^t s^{\mathscr{E}-1}f(s)ds \tag{27}$$

are referred to as fractal-fractional integral operators. These operators are mathematical tools that extend the concepts of differentiation and integration to non-integer orders. Fractal-fractional integral operators offer a robust framework for analyzing complex systems characterized by self-similarity or long-range dependencies. By integrating fractal geometry into traditional calculus, these operators provide a deeper understanding of phenomena that display intricate patterns across various scales. In essence, they bridge the gap between classical calculus and the complex dynamics observed in many real-world systems, paving the way for new analytical and interpretative approaches. Consequently, the proposed nonlinear fractional model, based on fractal-fractional operators, is presented with the help of system (1) as follows:

$$\left.\begin{aligned} {}_0^{FF}D_{0,t}^{\mathscr{E},\hbar}S_h(t) &= \psi_h + \omega_hR_h(t) - \frac{\delta\beta_h(1-\nu)S_h(t)I_m(t)}{1+\alpha_hI_m(t)} - \mu_hS_h(t) \\ {}_0^{FF}D_{0,t}^{\mathscr{E},\hbar}E_h(t) &= \frac{\delta\beta_h(1-\nu)S_h(t)I_m(t)}{1+\alpha_hI_m(t)} - \left(\mu_h+\gamma_h\right)E_h(t) \\ {}_0^{FF}D_{0,t}^{\mathscr{E},\hbar}I_h(t) &= \gamma_hE_h(t) + \varepsilon_hT_h(t) - \left(\mu_h+\phi_h+\sigma_h\right)I_h(t) \\ {}_0^{FF}D_{0,t}^{\mathscr{E},\hbar}T_h(t) &= \phi_hI_h(t) - \left(\mu_h+\varepsilon_h+\pi_h\right)T_h(t) \\ {}_0^{FF}D_{0,t}^{\mathscr{E},\hbar}R_h(t) &= \pi_hT_h(t) - \left(\mu_h+\omega_h\right)R_h(t) \\ {}_0^{FF}D_{0,t}^{\mathscr{E},\hbar}S_m(t) &= \rho(1-\varphi) - \left(\mu_m+\eta\tau\right)S_m(t) - \frac{\delta\beta_m(1-\nu)S_m(t)I_h(t)}{1+\alpha_mI_h(t)} \\ {}_0^{FF}D_{0,t}^{\mathscr{E},\hbar}E_m(t) &= \frac{\delta\beta_m(1-\nu)S_m(t)I_h(t)}{1+\alpha_mI_h(t)} - \left(\mu_m+\xi_m+\eta\tau\right)E_m(t) \\ {}_0^{FF}D_{0,t}^{\mathscr{E},\hbar}I_m(t) &= \xi_mE_m(t) - \left(\mu_m+\eta\tau+\sigma_m\right)I_m(t) \end{aligned}\right\} \tag{28}$$

We have ${}_0^{FF}D_{0,t}^{\mathscr{E},\hbar}(\cdot)$ as the fractal fractional derivative of order $0 < \mathscr{E} \leq 1$ and fractal dimension $0 < \hbar \leq 1$ in Caputo–Fabrizio sense with exponential law, and the variables with the appropriate initial conditions are supposed to be non-negative.

Lemma 1. *Let f be continuous on any open interval (x, y), then the following fractal fractional derivative*

$${}_0^{FF}D_{0,t}^{\mathscr{E},\hbar}(f(t)) = \mathcal{Q}(t) \tag{29}$$

has a unique solution

$$f(t) = f(0) + \frac{\hbar(1-\mathscr{E})t^{\hbar-1}f(t)}{\mathcal{P}(\mathscr{E})} + \frac{\mathscr{E}\hbar}{\mathcal{P}(\mathscr{E})}\int_0^t s^{\mathscr{E}-1}f(s)ds \tag{30}$$

For $\mathcal{U} = C\left(\mathscr{r}, \mathbb{R}^8\right)$, under the norm for $0 \leq t \leq t_f < \infty$ the Banach space represented by $\mathcal{B} = \mathcal{U}\times\mathcal{U}\times\mathcal{U}\times\mathcal{U}\times\mathcal{U}\times\mathcal{U}\times\mathcal{U}\times\mathcal{U}$ under the norm given by

$$\|M\| = sup_{t\in r}|M(t)| \qquad \text{for} \quad M \in U$$

where $|\mathcal{M}(t)| = \left|S_h + E_h + I_h + T_h + R_h + S_m + E_m + I_m\right|$, and $S_h, E_h, I_h, T_h, R_h, S_m, E_m, I_m \in C\left(\mathscr{r}, \mathbb{R}^8\right)$.

Therefore, the model system (28) can be transformed into the following:

$$\left.\begin{aligned} {}_0^{FFCF}D_{0,t}^{\mathscr{E}}\{S_h(t)\} &= \hbar t^{\hbar-1}\mathcal{W}_1\left(t, S_h(t)\right), & {}_0^{FFCF}D_{0,t}^{\mathscr{E}}\{E_h(t)\} &= \hbar t^{\hbar-1}\mathcal{W}_2\left(t, E_h(t)\right) \\ {}_0^{FFCF}D_{0,t}^{\mathscr{E}}\{I_h(t)\} &= \hbar t^{\hbar-1}\mathcal{W}_3\left(t, I_h(t)\right), & {}_0^{FFCF}D_{0,t}^{\mathscr{E}}\{T_h(t)\} &= \hbar t^{\hbar-1}\mathcal{W}_4\left(t, T_h(t)\right) \\ {}_0^{FFCF}D_{0,t}^{\mathscr{E}}\{R_h(t)\} &= \hbar t^{\hbar-1}\mathcal{W}_5\left(t, R_h(t)\right), & {}_0^{FFCF}D_{0,t}^{\mathscr{E}}\{S_m(t)\} &= \hbar t^{\hbar-1}\mathcal{W}_6\left(t, S_m(t)\right) \\ {}_0^{FFCF}D_{0,t}^{\mathscr{E}}\{E_m(t)\} &= \hbar t^{\hbar-1}\mathcal{W}_7\left(t, E_m(t)\right), & {}_0^{FFCF}D_{0,t}^{\mathscr{E}}\{I_m(t)\} &= \hbar t^{\hbar-1}\mathcal{W}_8\left(t, I_m(t)\right) \end{aligned}\right\}$$

where

$$\left.\begin{aligned} \mathcal{W}_1\left(t, S_h(t)\right) &= \psi_h + \omega_hR_h(t) - \frac{\delta\beta_h(1-\nu)S_h(t)I_m(t)}{1+\alpha_hI_m(t)} - \mu_hS_h(t) \\ \mathcal{W}_2\left(t, E_h(t)\right) &= \frac{\delta\beta_h(1-\nu)S_h(t)I_m(t)}{1+\alpha_hI_m(t)} - \left(\mu_h+\gamma_h\right)E_h(t) \\ \mathcal{W}_3\left(t, I_h(t)\right) &= \gamma_hE_h(t) + \varepsilon_hT_h(t) - \left(\mu_h+\phi_h+\sigma_h\right)I_h(t) \\ \mathcal{W}_4\left(t, T_h(t)\right) &= \phi_hI_h(t) - \left(\mu_h+\varepsilon_h+\pi_h\right)T_h(t) \\ \mathcal{W}_5\left(t, R_h(t)\right) &= \pi_hT_h(t) - \left(\mu_h+\omega_h\right)R_h(t) \\ \mathcal{W}_6\left(t, S_m(t)\right) &= \rho(1-\varphi) - \left(\mu_m+\eta\tau\right)S_m(t) - \frac{\delta\beta_m(1-\nu)S_m(t)I_h(t)}{1+\alpha_mI_h(t)} \\ \mathcal{W}_7\left(t, E_m(t)\right) &= \frac{\delta\beta_m(1-\nu)S_m(t)I_h(t)}{1+\alpha_mI_h(t)} - \left(\mu_m+\xi_m+\eta\tau\right)E_m(t) \\ \mathcal{W}_8\left(t, I_m(t)\right) &= \xi_mE_m(t) - \left(\mu_m+\eta\tau+\sigma_m\right)I_m(t) \end{aligned}\right\} \tag{31}$$

Introducing Caputo–Fabrizio integral in the system (31), we obtain the following:

$$\left.\begin{aligned}
S_h(t) &= S_h(0) + \frac{\hbar(1-\mathscr{b})t^{\hbar-1}}{\mathcal{P}(\mathscr{b})}\mathcal{W}_1\big(t, S_h(t)\big) + \frac{\mathscr{b}\hbar}{\mathcal{P}(\mathscr{b})}\int_0^t \varrho^{\mathscr{b}-1}\mathcal{W}_1\big(\varrho, S_h(\varrho)\big)d\varrho\\
E_h(t) &= E_h(0) + \frac{\hbar(1-\mathscr{b})t^{\hbar-1}}{\mathcal{P}(\mathscr{b})}\mathcal{W}_2\big(t, E_h(t)\big) + \frac{\mathscr{b}\hbar}{\mathcal{P}(\mathscr{b})}\int_0^t \varrho^{\mathscr{b}-1}\mathcal{W}_2\big(\varrho, E_h(\varrho)\big)d\varrho\\
I_h(t) &= I_h(0) + \frac{\hbar(1-\mathscr{b})t^{\hbar-1}}{\mathcal{P}(\mathscr{b})}\mathcal{W}_3\big(t, I_h(t)\big) + \frac{\mathscr{b}\hbar}{\mathcal{P}(\mathscr{b})}\int_0^t \varrho^{\mathscr{b}-1}\mathcal{W}_3\big(\varrho, I_h(\varrho)\big)d\varrho\\
T_h(t) &= T_h(0) + \frac{\hbar(1-\mathscr{b})t^{\hbar-1}}{\mathcal{P}(\mathscr{b})}\mathcal{W}_4\big(t, T_h(t)\big) + \frac{\mathscr{b}\hbar}{\mathcal{P}(\mathscr{b})}\int_0^t \varrho^{\mathscr{b}-1}\mathcal{W}_4\big(\varrho, T_h(\varrho)\big)d\varrho\\
R_h(t) &= R_h(0) + \frac{\hbar(1-\mathscr{b})t^{\hbar-1}}{\mathcal{P}(\mathscr{b})}\mathcal{W}_5\big(t, R_h(t)\big) + \frac{\mathscr{b}\hbar}{\mathcal{P}(\mathscr{b})}\int_0^t \varrho^{\mathscr{b}-1}\mathcal{W}_5\big(\varrho, R_h(\varrho)\big)d\varrho\\
S_m(t) &= S_m(0) + \frac{\hbar(1-\mathscr{b})t^{\hbar-1}}{\mathcal{P}(\mathscr{b})}\mathcal{W}_6\big(t, S_m(t)\big) + \frac{\mathscr{b}\hbar}{\mathcal{P}(\mathscr{b})}\int_0^t \varrho^{\mathscr{b}-1}\mathcal{W}_6\big(\varrho, S_m(\varrho)\big)d\varrho\\
E_m(t) &= E_m(0) + \frac{\hbar(1-\mathscr{b})t^{\hbar-1}}{\mathcal{P}(\mathscr{b})}\mathcal{W}_7\big(t, E_m(t)\big) + \frac{\mathscr{b}\hbar}{\mathcal{P}(\mathscr{b})}\int_0^t \varrho^{\mathscr{b}-1}\mathcal{W}_7\big(\varrho, E_m(\varrho)\big)d\varrho\\
I_m(t) &= I_m(0) + \frac{\hbar(1-\mathscr{b})t^{\hbar-1}}{\mathcal{P}(\mathscr{b})}\mathcal{W}_8\big(t, I_m(t)\big) + \frac{\mathscr{b}\hbar}{\mathcal{P}(\mathscr{b})}\int_0^t \varrho^{\mathscr{b}-1}\mathcal{W}_8\big(\varrho, I_m(\varrho)\big)d\varrho
\end{aligned}\right\} \tag{32}$$

The Picard–Lindel'f method and the fixed-point theory will be used to illustrate the qualitative characteristics of the solution for the model system (28). Therefore, we rewrite the model system (28) and get the following;

$$\left.\begin{aligned}
&{}_0^{FF}D_{0,t}^{\mathscr{b},\hbar}\,\mathcal{M}(t) = \mathcal{W}(t, \mathcal{M}(t)), && 0 < \mathscr{b}, \hbar \le 1\\
&\mathcal{M}(0) = \mathcal{M}_0 \ge 0, && t \in [0, t_f] \text{ and } (t_f < \infty)
\end{aligned}\right\} \tag{33}$$

$$\mathcal{M}(t) = \begin{pmatrix} S_h(t)\\ E_h(t)\\ I_h(t)\\ T_h(t)\\ R_h(t)\\ S_m(t)\\ E_m(t)\\ I_m(t)\end{pmatrix},\quad \mathcal{M}(0) = \begin{pmatrix} S_h(0)=S_{h0}\\ E_h(0)=E_{h0}\\ I_h(0)=I_{h0}\\ T_h(0)=T_{h0}\\ R_h(0)=R_{h0}\\ S_m(0)=S_{m0}\\ E_m(0)=E_{m0}\\ I_m(0)=I_{m0}\end{pmatrix} = \mathcal{M}_0,\quad \mathcal{W}(t, \mathcal{M}(t)) = \begin{pmatrix} \mathcal{W}_1(t, S_h(t))\\ \mathcal{W}_2(t, E_h(t))\\ \mathcal{W}_3(t, I_h(t))\\ \mathcal{W}_4(t, T_h(t))\\ \mathcal{W}_5(t, R_h(t))\\ \mathcal{W}_6(t, S_m(t))\\ \mathcal{W}_7(t, E_m(t))\\ \mathcal{W}_8(t, I_m(t))\end{pmatrix}$$

From Lemma 1, we have system (33) as

$$\mathcal{M}(t) = \mathcal{M}(0) + \frac{\hbar(1-\mathscr{b})t^{\hbar-1}}{\mathcal{P}(\mathscr{b})}\mathcal{W}(t, \mathcal{M}(t)) + \frac{\mathscr{b}\hbar}{\mathcal{P}(\mathscr{b})}\int_0^t \varrho^{\mathscr{b}-1}\mathcal{W}(\varrho, \mathcal{M}(\varrho))d\varrho$$

Consequently, $\mathcal{W}$ satisfies

$$\Big\|\mathcal{M}\big(\varrho, \mathcal{W}_1(\varrho)\big) - \mathcal{M}\big(\varrho, \mathcal{W}_2(\varrho)\big)\Big\| \le \mathcal{K}_{\mathcal{W}}\big|\mathcal{W}_1(\varrho) - \mathcal{W}_2(\varrho)\big|, \qquad \mathcal{K}_{\mathcal{W}} > 0 \tag{34}$$

Theorem 3. *If the assumption of System* (34) *holds, that is,* $\mathbb{P} = \left(\frac{\hbar(1-\mathscr{b})t_f^{\hbar-1}}{\mathcal{P}(\mathscr{b})} + \frac{\mathscr{b}\hbar t_f^{\hbar}}{\mathcal{P}(\mathscr{b})}\right)\mathcal{K}_{\mathcal{W}} \le 1$, *we assume that system* (33) *has a unique solution.*

Proof. Let us consider the Picard operator denoted by the symbol $\Delta : \mathcal{U} \longrightarrow \mathcal{U}$, with the definition

$$\Delta\mathcal{M}(t) = \mathcal{M}(0) + \frac{\hbar(1-\mathscr{b})t^{\hbar-1}}{\mathcal{P}(\mathscr{b})}\mathcal{W}(t, \mathcal{M}(t)) + \frac{\mathscr{b}\hbar}{\mathcal{P}(\mathscr{b})}\int_0^t \varrho^{\mathscr{b}-1}\mathcal{W}(\varrho, \mathcal{M}(\varrho))d\varrho \tag{35}$$

Finally, we set $sup_{t\in r}\mathcal{W}(\varrho, 0) = \mathcal{W}_0$. Therefore, it is important to note that the solution of system (33) is constrained, that is,

$$\begin{aligned}
\|\Delta\mathcal{M} - \mathcal{M}_0\| &= sup_{t\in r}|\Delta\mathcal{M} - \mathcal{M}_0|\\
&= sup_{t\in r}\left|\frac{\hbar(1-\mathscr{b})t^{\hbar-1}}{\mathcal{P}(\mathscr{b})}\mathcal{W}(t, \mathcal{M}(t)) + \frac{\mathscr{b}\hbar}{\mathcal{P}(\mathscr{b})}\int_0^t \varrho^{\mathscr{b}-1}\mathcal{W}(\varrho, \mathcal{M}(\varrho))d\varrho\right|\\
&\le sup_{t\in r}\left|\frac{\hbar(1-\mathscr{b})t^{\hbar-1}}{\mathcal{P}(\mathscr{b})}\mathcal{W}(t, \mathcal{M}(t)) + \frac{\mathscr{b}\hbar}{\mathcal{P}(\mathscr{b})}\int_0^t \varrho^{\mathscr{b}-1}\mathcal{W}(\varrho, \mathcal{M}(\varrho))d\varrho\right|\\
&\le sup_{t\in r}\left(\frac{\hbar(1-\mathscr{b})t_f^{\hbar-1}}{\mathcal{P}(\mathscr{b})} + \frac{\mathscr{b}\hbar t_f^{\hbar}}{\mathcal{P}(\mathscr{b})}\right)\mathcal{K}_{\mathcal{W}}, \le \left(\frac{\hbar(1-\mathscr{b})t_f^{\hbar-1}}{\mathcal{P}(\mathscr{b})} + \frac{\mathscr{b}\hbar t_f^{\hbar}}{\mathcal{P}(\mathscr{b})}\right)\\
&\mathcal{K}_{\mathcal{W}} \le \vartheta\mathcal{K}_{\mathcal{W}}
\end{aligned}$$

where $\vartheta\mathcal{K}_{\mathcal{W}} < 1$. Consequently, from the definition of the Picard operator in the system (35) for any $\mathcal{M}_1, \mathcal{M}_2 \in \mathcal{U}$, we have

$$\begin{aligned}
\|\Delta\mathcal{M}_1 - \Delta\mathcal{M}_2\| &= sup_{t\in r}|\Delta\mathcal{M}_1(t) - \Delta\mathcal{M}_2(t)|\\
&= sup_{t\in r}\frac{\hbar(1-\mathscr{b})t^{\hbar-1}}{\mathcal{P}(\mathscr{b})}\Big\|\mathcal{W}(t, \mathcal{M}_1(t)) - \mathcal{W}(t, \mathcal{M}_2(t))\Big\| + \frac{\mathscr{b}\hbar}{\mathcal{P}(\mathscr{b})}\int_0^t \varrho^{\mathscr{b}-1}\\
&\Big\|\mathcal{W}(\varrho, \mathcal{M}_1(\varrho)) - \mathcal{W}(\varrho, \mathcal{M}_2(\varrho))\Big\|d\varrho\\
&\le sup_{t\in r}\frac{\hbar(1-\mathscr{b})t^{\hbar-1}}{\mathcal{P}(\mathscr{b})}\mathcal{K}_{\mathcal{W}}|\mathcal{M}_1(t) - \mathcal{M}_2(t)| + \frac{\mathscr{b}\hbar}{\mathcal{P}(\mathscr{b})}\int_0^t \varrho^{\mathscr{b}-1}\mathcal{K}_{\mathcal{W}}\\
&|\mathcal{M}_1(\varrho) - \mathcal{M}_2(\varrho)|d\varrho\\
&\le sup_{t\in r}\left(\frac{\hbar(1-\mathscr{b})t_f^{\hbar-1}}{\mathcal{P}(\mathscr{b})} + \frac{\mathscr{b}\hbar t_f^{\hbar}}{\mathcal{P}(\mathscr{b})}\right)\mathcal{K}_{\mathcal{W}}, \le \left(\frac{\hbar(1-\mathscr{b})t_f^{\hbar-1}}{\mathcal{P}(\mathscr{b})} + \frac{\mathscr{b}\hbar t_f^{\hbar}}{\mathcal{P}(\mathscr{b})}\right)\mathcal{K}_{\mathcal{W}} \le \vartheta\mathcal{K}_{\mathcal{W}}
\end{aligned}$$

This implies that $\|\Delta\mathcal{M}_1 - \Delta\mathcal{M}_2\| \le \mathbb{P}\|\mathcal{M}_1 - \mathcal{M}_2\|$. As $\mathbb{P}$ is a contraction, the model system (33) has a unique solution under the Banach contraction principle. □

Definition 3. Suppose that $\mathcal{W} \in C\big(r \times \mathbb{R}^8, \mathbb{R}\big)$, then for $0 < \mathscr{b}, \hbar \le 1$ system (29) is said to be Hyers–Ulam–Rassias stable if there exists $C_{\mathcal{W},,F} > 0$ such that, for each solution $\widehat{\mathcal{Q}} \in \mathcal{U}$ satisfies

$$\left\|{}_0^{FF}D_{0,t}^{\mathscr{b},\hbar}\,\widehat{\mathcal{Q}}(t) - \mathcal{W}(t, \widehat{\mathcal{Q}}(t))\right\| \le \Pi F(t)^{t_f}, \qquad \text{for all } t \in r \tag{36}$$

There exists a solution $\mathcal{Q} \in \mathcal{U}$ of the system (29) with

$$|\,\widehat{\mathcal{Q}}(t) - \mathcal{Q}(t)| \le C_{\mathcal{W},,F}F(t) \qquad \text{for all } t \in r \tag{37}$$

where $C_{\mathcal{W},,F} = max\big(C_{\mathcal{W},,F}\big)^{t_f}$ and $F = max\big(F_i\big)^{t_f}$, $i = 1, 2, \ldots, 8$.

Lemma 2. *If* $\Pi > 0$ *and if there exists a function* $\ell(t) \in \mathcal{U}$ *which satisfies*

(i) $l^*(t) \le \Pi$, *for all* $t \in r$

(ii) ${}_0^{FF}D_{0,t}^{\mathscr{b},\hbar}\,\widehat{\mathcal{Q}}(t) = \mathcal{W}(t, \widehat{\mathcal{Q}}(t)) + \ell^*(t)$, *for all* $t \in r$ $\ell^* = max\big(\ell_i^*\big)^{t_f}, i = 1, 2, \ldots, 8$

then the function $\widehat{\mathcal{Q}} \in \mathcal{U}$ *satisfies the system* (36).

3.2 | Hyers-Ulam Stability Analysis

We shall at this point use the Hyers-Ulam and Hyers-Ulam-Rassias stability to examine the stability of the model.

Lemma 3. *If* $\mathcal{M}$ *satisfies the integral inequality given in the system* (38), *then* $\mathcal{M} \in \mathcal{U}$ *satisfies the system* (33).

$$\left|\mathcal{M}(t) - \mathcal{M}_0 - \frac{\hbar(1-\mathscr{b})t^{\hbar-1}}{\mathcal{P}(\mathscr{b})}\mathcal{W}(\varrho, \mathcal{M}(\varrho)) + \frac{\mathscr{b}\hbar}{\mathcal{P}(\mathscr{b})}\int_0^t \varrho^{\mathscr{b}-1}\mathcal{W}(\varrho, \mathcal{M}(\varrho))d\varrho\right| \le \Theta\Pi \tag{38}$$

where $\Theta = \left(\frac{\hbar(1-\mathscr{b})t_f^{\hbar-1}}{\mathcal{P}(\mathscr{b})} + \frac{\mathscr{b}\hbar t_f^{\hbar}}{\mathcal{P}(\mathscr{b})}\right)$.

Proof. From (ii) of Lemma 2, we have that system (38) exists; that is,

$${}_0^{FF}D_{0,t}^{\mathscr{b},\hbar}\,\mathcal{M}(t) = \mathcal{W}(t, \mathcal{M}(t)) + f(t) \qquad t \in r$$
$$\mathcal{M}(0) = \mathcal{M}_0 \ge 0$$

and has a unique solution

$$\mathcal{M}(t) = \mathcal{M}_0 + \frac{\hbar(1-\mathscr{b})t^{\hbar-1}}{\mathcal{P}(\mathscr{b})}(\mathcal{W}(\varrho, \mathcal{M}(\varrho)) + f(t)) + \frac{\mathscr{b}\hbar}{\mathcal{P}(\mathscr{b})}\int_0^t \varrho^{\mathscr{b}-1}(\mathcal{W}(\varrho, \mathcal{M}(\varrho)) + f(t))d\varrho$$

□

It continues to follow from (i) of Lemma 2 that:

$$\left|\mathcal{M}(t)=\mathcal{M}_0+\frac{\hbar(1-\mathscr{b})t^{\hbar-1}}{\mathcal{P}(\mathscr{b})}\mathcal{W}(\mathscr{q},\mathcal{M}(\mathscr{q}))+\frac{\mathscr{b}\hbar}{\mathcal{P}(\mathscr{b})}\int_0^t \mathscr{q}^{\mathscr{b}-1}\mathcal{W}(\mathscr{q},\mathcal{M}(\mathscr{q}))d\mathscr{q}\right|$$
$$=sup_{t\in\mathscr{r}}\left|\frac{\hbar(1-\mathscr{b})t^{\hbar-1}}{\mathcal{P}(\mathscr{b})}f(t)+\frac{\mathscr{b}\hbar}{\mathcal{P}(\mathscr{b})}\int_0^t \mathscr{q}^{\mathscr{b}-1}\mathcal{W}f(t)d\mathscr{q}\right|\leq sup_{t\in\mathscr{r}}\frac{\hbar(1-\mathscr{b})t^{\hbar-1}}{\mathcal{P}(\mathscr{b})}+\frac{\mathscr{b}\hbar}{\mathcal{P}(\mathscr{b})}\int_0^t \mathscr{q}^{\mathscr{b}-1}d\mathscr{q}$$
$$\leq sup_{t\in\mathscr{r}}\left(\frac{\hbar(1-\mathscr{b})t^{\hbar-1}}{\mathcal{P}(\mathscr{b})}+\frac{\mathscr{b}\hbar}{\mathcal{P}(\mathscr{b})}\int_0^t \mathscr{q}^{\mathscr{b}-1}d\mathscr{q}\right),\leq\left(\frac{\hbar(1-\mathscr{b})t_f^{\hbar-1}}{\mathcal{P}(\mathscr{b})}+\frac{\mathscr{b}\hbar t_f^{\hbar}}{\mathcal{P}(\mathscr{b})}\right)\Pi\leq\Theta\Pi$$

Theorem 4. *Suppose that* $\mathcal{W}\in C\left(\mathscr{r}\times\mathbb{R}^8,\mathbb{R}\right)$ *and the system* (34) *satisfies condition* $1-\Theta\mathcal{K}_{\mathcal{W}}>0$, *then the system* (33) *is said to be Hyers–Ulam stable.*

Proof. Let $\mathcal{M}\in\mathcal{U}$ be a unique solution for the system (33) and $\widehat{\mathcal{M}}\in\mathcal{U}$ by (36). Then, by taking Lemma 2 into consideration, for any $\Pi>0, t\in\mathscr{r}$ we have

$$\|\widehat{\mathcal{M}}-\mathcal{M}\|=sup_{t\in\mathscr{r}}|\widehat{\mathcal{M}}-\mathcal{M}|$$
$$=sup_{t\in\mathscr{r}}\left|\widehat{\mathcal{M}}-\mathcal{M}_0-\frac{\hbar(1-\mathscr{b})t^{\hbar-1}}{\mathcal{P}(\mathscr{b})}\mathcal{W}(\mathscr{q},\mathcal{M}(\mathscr{q}))-\frac{\mathscr{b}\hbar}{\mathcal{P}(\mathscr{b})}\int_0^t \mathscr{q}^{\mathscr{b}-1}\mathcal{W}(\mathscr{q},\mathcal{M}(\mathscr{q}))d\mathscr{q}\right|$$
$$\leq sup_{t\in\mathscr{r}}\left|\widehat{\mathcal{M}}-\mathcal{M}_0-\frac{\hbar(1-\mathscr{b})t^{\hbar-1}}{\mathcal{P}(\mathscr{b})}\mathcal{W}(\mathscr{q},\widehat{\mathcal{M}}(\mathscr{q}))-\frac{\mathscr{b}\hbar}{\mathcal{P}(\mathscr{b})}\int_0^t \mathscr{q}^{\mathscr{b}-1}\mathcal{W}(\mathscr{q},\widehat{\mathcal{M}}(\mathscr{q}))d\mathscr{q}\right|$$
$$+sup_{t\in\mathscr{r}}\left|\frac{\hbar(1-\mathscr{b})t^{\hbar-1}}{\mathcal{P}(\mathscr{b})}(\mathcal{W}(\mathscr{q},\widehat{\mathcal{M}}(\mathscr{q}))-\mathcal{W}(\mathscr{q},\mathcal{M}(\mathscr{q})))-\frac{\mathscr{b}\hbar}{\mathcal{P}(\mathscr{b})}\int_0^t \mathscr{q}^{\mathscr{b}-1}(\mathcal{W}(\mathscr{q},\widehat{\mathcal{M}}(\mathscr{q}))\right.$$
$$\left.-\mathcal{W}(\mathscr{q},\mathcal{M}(\mathscr{q})))d\mathscr{q}\right|$$
$$\leq\Theta\Pi+sup_{t\in\mathscr{r}}\left(\frac{\hbar(1-\mathscr{b})t^{\hbar-1}}{\mathcal{P}(\mathscr{b})}|\mathcal{W}(\mathscr{q},\widehat{\mathcal{M}}(\mathscr{q}))-\mathcal{W}(\mathscr{q},\mathcal{M}(\mathscr{q}))|-\frac{\mathscr{b}\hbar}{\mathcal{P}(\mathscr{b})}\int_0^t \mathscr{q}^{\mathscr{b}-1}|\mathcal{W}(\mathscr{q},\widehat{\mathcal{M}}(\mathscr{q}))\right.$$
$$\left.-\mathcal{W}(\mathscr{q},\mathcal{M}(\mathscr{q}))|d\mathscr{q}\right)$$
$$\leq\Theta\Pi+sup_{t\in\mathscr{r}}\left(\frac{\hbar(1-\mathscr{b})t^{\hbar-1}}{\mathcal{P}(\mathscr{b})}\mathcal{K}_{\mathcal{W}}|\widehat{\mathcal{M}}(\mathscr{q})-\mathcal{M}(\mathscr{q})|-\frac{\mathscr{b}\hbar}{\mathcal{P}(\mathscr{b})}\int_0^t \mathscr{q}^{\mathscr{b}-1}\mathcal{K}_{\mathcal{W}}|\widehat{\mathcal{M}}(\mathscr{q})-\mathcal{M}(\mathscr{q})|d\mathscr{q}\right)$$
$$\leq\Theta\Pi+sup_{t\in\mathscr{r}}\left(\frac{\hbar(1-\mathscr{b})t^{\hbar-1}}{\mathcal{P}(\mathscr{b})}-\frac{\mathscr{b}\hbar}{\mathcal{P}(\mathscr{b})}\int_0^t \mathscr{q}^{\mathscr{b}-1}\right)\mathcal{K}_{\mathcal{W}}|\widehat{\mathcal{M}}(\mathscr{q})-\mathcal{M}(\mathscr{q})|$$
$$\leq\Theta\Pi+sup_{t\in\mathscr{r}}\left(\frac{\hbar(1-\mathscr{b})t_f^{\hbar-1}}{\mathcal{P}(\mathscr{b})}-\frac{\mathscr{b}\hbar t_f^{\hbar}}{\mathcal{P}(\mathscr{b})}\right)\mathcal{K}_{\mathcal{W}}|\widehat{\mathcal{M}}(\mathscr{q})-\mathcal{M}(\mathscr{q})|\leq\Theta\Pi+\Theta\mathcal{K}_{\mathcal{W}}\|\widehat{\mathcal{M}}-\mathcal{M}\|$$

□

Which implies that

$$\|\widehat{\mathcal{M}}-\mathcal{M}\|\leq C_{\mathcal{W}}\Pi$$

where $C_{\mathcal{W}}=\frac{\Theta}{1-\Theta\mathcal{K}_{\mathcal{W}}}$.

Theorem 5. *Suppose that* $\mathcal{W}\in C\left(\mathscr{r}\times\mathbb{R}^8,\mathbb{R}\right)$ *satisfies system* (34) *and* $F\in C\left(\mathscr{r}\times\mathbb{R}^+\right)$ *be an increasing function implies that the system* (33) *is Hyers-Ulam-Rassias stable concerning Fon* $\mathscr{r}$, *such that*

$$_0^{FF}D_{0,t}^{\mathscr{b},\hbar}F(t)\leq C_F F(t),\qquad C_F>0\tag{39}$$

provided that $1-\Theta\mathcal{K}_{\mathcal{W}}>0$.

Proof. We assume that there exists exactly one solution $\mathcal{M}\in\mathcal{U}$ to the system (33). Thus, with

$$\mathcal{M}(t)=\mathcal{M}_0+\frac{\hbar(1-\mathscr{b})t^{\hbar-1}}{\mathcal{P}(\mathscr{b})}\mathcal{W}(t,\mathcal{M}(t))+\frac{\mathscr{b}\hbar}{\mathcal{P}(\mathscr{b})}\int_0^t \mathscr{q}^{\mathscr{b}-1}\mathcal{W}(\mathscr{q},\mathcal{M}(\mathscr{q}))d\mathscr{q}$$

□

Thus, considering system (36), we obtain

$$\left|\mathcal{M}(t)-\mathcal{M}_0-\frac{\hbar(1-\mathscr{b})t^{\hbar-1}}{\mathcal{P}(\mathscr{b})}\mathcal{W}(t,\mathcal{M}(t))-\frac{\mathscr{b}\hbar}{\mathcal{P}(\mathscr{b})}\int_0^t \mathscr{q}^{\mathscr{b}-1}\mathcal{W}(\mathscr{q},\mathcal{M}(\mathscr{q}))d\mathscr{q}\right|\leq\Pi C_F F(t)$$

This gives

$$|\widehat{\mathcal{M}}-\mathcal{M}|=sup_{t\in\mathscr{r}}\left|\widehat{\mathcal{M}}(t)-\mathcal{M}_0-\frac{\hbar(1-\mathscr{b})t^{\hbar-1}}{\mathcal{P}(\mathscr{b})}\mathcal{W}(t,\mathcal{M}(t))-\frac{\mathscr{b}\hbar}{\mathcal{P}(\mathscr{b})}\int_0^t \mathscr{q}^{\mathscr{b}-1}\mathcal{W}(\mathscr{q},\mathcal{M}(\mathscr{q}))d\mathscr{q}\right|$$
$$\leq sup_{t\in\mathscr{r}}\left|\widehat{\mathcal{M}}(t)-\mathcal{M}_0-\frac{\hbar(1-\mathscr{b})t^{\hbar-1}}{\mathcal{P}(\mathscr{b})}\mathcal{W}(t,\widehat{\mathcal{M}}(t))-\frac{\mathscr{b}\hbar}{\mathcal{P}(\mathscr{b})}\int_0^t \mathscr{q}^{\mathscr{b}-1}\mathcal{W}(\mathscr{q},\widehat{\mathcal{M}}(\mathscr{q}))d\mathscr{q}\right|$$
$$+sup_{t\in\mathscr{r}}\left|\frac{\hbar(1-\mathscr{b})t^{\hbar-1}}{\mathcal{P}(\mathscr{b})}(\mathcal{W}(t,\widehat{\mathcal{M}}(t))-\mathcal{W}(t,\mathcal{M}(t)))-\frac{\mathscr{b}\hbar}{\mathcal{P}(\mathscr{b})}\int_0^t \mathscr{q}^{\mathscr{b}-1}(\mathcal{W}(t,\widehat{\mathcal{M}}(t))-\mathcal{W}(t,\mathcal{M}(t)))d\mathscr{q}\right|$$
$$\leq\Pi C_F F(t)+sup_{t\in\mathscr{r}}\left(\frac{\hbar(1-\mathscr{b})t^{\hbar-1}}{\mathcal{P}(\mathscr{b})}|\mathcal{W}(t,\widehat{\mathcal{M}}(t))-\mathcal{W}(t,\mathcal{M}(t))|-\frac{\mathscr{b}\hbar}{\mathcal{P}(\mathscr{b})}\int_0^t \mathscr{q}^{\mathscr{b}-1}|\mathcal{W}(t,\widehat{\mathcal{M}}(t))\right.$$
$$\left.-\mathcal{W}(t,\mathcal{M}(t))|d\mathscr{q}\right)$$
$$\leq\Pi C_F F(t)+sup_{t\in\mathscr{r}}\left(\frac{\hbar(1-\mathscr{b})t^{\hbar-1}}{\mathcal{P}(\mathscr{b})}\mathcal{K}_{\mathcal{W}}|\widehat{\mathcal{M}}(t)-\mathcal{M}(t)|-\frac{\mathscr{b}\hbar}{\mathcal{P}(\mathscr{b})}\int_0^t \mathscr{q}^{\mathscr{b}-1}\mathcal{K}_{\mathcal{W}}|\widehat{\mathcal{M}}(t)-\mathcal{M}(t)|d\mathscr{q}\right)$$
$$\leq\Pi C_F F(t)+sup_{t\in\mathscr{r}}\left(\frac{\hbar(1-\mathscr{b})t^{\hbar-1}}{\mathcal{P}(\mathscr{b})}-\frac{\mathscr{b}\hbar}{\mathcal{P}(\mathscr{b})}\int_0^t \mathscr{q}^{\mathscr{b}-1}d\mathscr{q}\right)\mathcal{K}_{\mathcal{W}}|\widehat{\mathcal{M}}(t)-\mathcal{M}(t)|$$
$$\leq\Pi C_F F(t)+\left(\frac{\hbar(1-\mathscr{b})t_f^{\hbar-1}}{\mathcal{P}(\mathscr{b})}-\frac{\mathscr{b}\hbar t_f^{\hbar}}{\mathcal{P}(\mathscr{b})}\right)\mathcal{K}_{\mathcal{W}}|\widehat{\mathcal{M}}(t)-\mathcal{M}(t)|\leq\Pi C_F F(t)+\Theta\mathcal{K}_{\mathcal{W}}|\widehat{\mathcal{M}}-\mathcal{M}|$$
$$|\widehat{\mathcal{M}}-\mathcal{M}|\leq\Pi C_{\mathcal{W},\ F}F(t)\tag{40}$$

where $C_{\mathcal{W},\ F}=\frac{C_F}{1-\Theta\mathcal{K}_{\mathcal{W}}}$.

4 | Numerical Algorithm

The numerical scheme developed for simulating the model system (28) is detailed in this section. At time step, t_{n+1}, we have:

$$\left.\begin{aligned}
S_h(t_{n+1})&=S_h(t_0)+\frac{\hbar(1-\mathscr{b})t_n^{\hbar-1}}{\mathcal{P}(\mathscr{b})}\mathcal{W}_1(t_n,S_h(t_n))+\frac{\mathscr{b}\hbar}{\mathcal{P}(\mathscr{b})}\int_0^t \mathscr{q}^{\mathscr{b}-1}\mathcal{W}_1(\mathscr{q},S_h(\mathscr{q}))d\mathscr{q}\\
E_h(t_{n+1})&=E_h(t_0)+\frac{\hbar(1-\mathscr{b})t_n^{\hbar-1}}{\mathcal{P}(\mathscr{b})}\mathcal{W}_2(t_n,E_h(t_n))+\frac{\mathscr{b}\hbar}{\mathcal{P}(\mathscr{b})}\int_0^t \mathscr{q}^{\mathscr{b}-1}\mathcal{W}_2(\mathscr{q},E_h(\mathscr{q}))d\mathscr{q}\\
I_h(t_{n+1})&=I_h(t_0)+\frac{\hbar(1-\mathscr{b})t_n^{\hbar-1}}{\mathcal{P}(\mathscr{b})}\mathcal{W}_3(t_n,I_h(t_n))+\frac{\mathscr{b}\hbar}{\mathcal{P}(\mathscr{b})}\int_0^t \mathscr{q}^{\mathscr{b}-1}\mathcal{W}_3(\mathscr{q},I_h(\mathscr{q}))d\mathscr{q}\\
T_h(t_{n+1})&=T_h(t_0)+\frac{\hbar(1-\mathscr{b})t_n^{\hbar-1}}{\mathcal{P}(\mathscr{b})}\mathcal{W}_4(t_n,T_h(t_n))+\frac{\mathscr{b}\hbar}{\mathcal{P}(\mathscr{b})}\int_0^t \mathscr{q}^{\mathscr{b}-1}\mathcal{W}_4(\mathscr{q},T_h(\mathscr{q}))d\mathscr{q}\\
R_h(t_{n+1})&=R_h(t_0)+\frac{\hbar(1-\mathscr{b})t_n^{\hbar-1}}{\mathcal{P}(\mathscr{b})}\mathcal{W}_5(t_n,R_h(t_n))+\frac{\mathscr{b}\hbar}{\mathcal{P}(\mathscr{b})}\int_0^t \mathscr{q}^{\mathscr{b}-1}\mathcal{W}_5(\mathscr{q},R_h(\mathscr{q}))d\mathscr{q}\\
S_m(t_{n+1})&=S_m(t_0)+\frac{\hbar(1-\mathscr{b})t_n^{\hbar-1}}{\mathcal{P}(\mathscr{b})}\mathcal{W}_6(t_n,S_m(t_n))+\frac{\mathscr{b}\hbar}{\mathcal{P}(\mathscr{b})}\int_0^t \mathscr{q}^{\mathscr{b}-1}\mathcal{W}_6(\mathscr{q},S_m(\mathscr{q}))d\mathscr{q}\\
E_m(t_{n+1})&=E_m(t_0)+\frac{\hbar(1-\mathscr{b})t_n^{\hbar-1}}{\mathcal{P}(\mathscr{b})}\mathcal{W}_7(t_n,E_m(t_n))+\frac{\mathscr{b}\hbar}{\mathcal{P}(\mathscr{b})}\int_0^t \mathscr{q}^{\mathscr{b}-1}\mathcal{W}_7(\mathscr{q},E_m(\mathscr{q}))d\mathscr{q}\\
I_m(t_{n+1})&=I_m(t_0)+\frac{\hbar(1-\mathscr{b})t_n^{\hbar-1}}{\mathcal{P}(\mathscr{b})}\mathcal{W}_8(t_n,I_m(t_n))+\frac{\mathscr{b}\hbar}{\mathcal{P}(\mathscr{b})}\int_0^t \mathscr{q}^{\mathscr{b}-1}\mathcal{W}_8(\mathscr{q},I_m(\mathscr{q}))d\mathscr{q}
\end{aligned}\right\}\tag{41}$$

If the gap between two successive terms is taken as a starting point, we obtain the following.

$$\left.\begin{aligned}
S_h(t_{n+1})&=S_h(t_n)+\frac{\hbar(1-\mathscr{b})t_n^{\hbar-1}}{\mathcal{P}(\mathscr{b})}\mathcal{W}_1(t_n,S_h(t_n))-\frac{\hbar(1-\mathscr{b})t_{n-1}^{\hbar-1}}{\mathcal{P}(\mathscr{b})}\mathcal{W}_1(t_{n-1},S_h(t_{n-1}))\\
&\quad+\frac{\mathscr{b}\hbar}{\mathcal{P}(\mathscr{b})}\int_{t_n}^{t_{n-1}} \mathscr{q}^{\mathscr{b}-1}\mathcal{W}_1(\mathscr{q},S_h(\mathscr{q}))d\mathscr{q},\\
E_h(t_{n+1})&=E_h(t_0)+\frac{\hbar(1-\mathscr{b})t_n^{\hbar-1}}{\mathcal{P}(\mathscr{b})}\mathcal{W}_2(t_n,E_h(t_n))-\frac{\hbar(1-\mathscr{b})t_{n-1}^{\hbar-1}}{\mathcal{P}(\mathscr{b})}\mathcal{W}_2(t_{n-1},E_h(t_{n-1}))\\
&\quad+\frac{\mathscr{b}\hbar}{\mathcal{P}(\mathscr{b})}\int_{t_n}^{t_{n-1}} \mathscr{q}^{\mathscr{b}-1}\mathcal{W}_2(\mathscr{q},E_h(\mathscr{q}))d\mathscr{q},\\
I_h(t_{n+1})&=I_h(t_0)+\frac{\hbar(1-\mathscr{b})t_n^{\hbar-1}}{\mathcal{P}(\mathscr{b})}\mathcal{W}_3(t_n,I_h(t_n))-\frac{\hbar(1-\mathscr{b})t_{n-1}^{\hbar-1}}{\mathcal{P}(\mathscr{b})}\mathcal{W}_3(t_{n-1},I_h(t_{n-1}))\\
&\quad+\frac{\mathscr{b}\hbar}{\mathcal{P}(\mathscr{b})}\int_{t_n}^{t_{n-1}} \mathscr{q}^{\mathscr{b}-1}\mathcal{W}_3(\mathscr{q},I_h(\mathscr{q}))d\mathscr{q},\\
T_h(t_{n+1})&=T_h(t_0)+\frac{\hbar(1-\mathscr{b})t_n^{\hbar-1}}{\mathcal{P}(\mathscr{b})}\mathcal{W}_4(t_n,T_h(t_n))-\frac{\hbar(1-\mathscr{b})t_{n-1}^{\hbar-1}}{\mathcal{P}(\mathscr{b})}\mathcal{W}_4(t_{n-1},T_h(t_{n-1}))\\
&\quad+\frac{\mathscr{b}\hbar}{\mathcal{P}(\mathscr{b})}\int_{t_n}^{t_{n-1}} \mathscr{q}^{\mathscr{b}-1}\mathcal{W}_4(\mathscr{q},T_h(\mathscr{q}))d\mathscr{q},\\
R_h(t_{n+1})&=R_h(t_0)+\frac{\hbar(1-\mathscr{b})t_n^{\hbar-1}}{\mathcal{P}(\mathscr{b})}\mathcal{W}_5(t_n,R_h(t_n))-\frac{\hbar(1-\mathscr{b})t_{n-1}^{\hbar-1}}{\mathcal{P}(\mathscr{b})}\mathcal{W}_5(t_{n-1},R_h(t_{n-1}))\\
&\quad+\frac{\mathscr{b}\hbar}{\mathcal{P}(\mathscr{b})}\int_{t_n}^{t_{n-1}} \mathscr{q}^{\mathscr{b}-1}\mathcal{W}_5(\mathscr{q},R_h(\mathscr{q}))d\mathscr{q},\\
S_m(t_{n+1})&=S_m(t_0)+\frac{\hbar(1-\mathscr{b})t_n^{\hbar-1}}{\mathcal{P}(\mathscr{b})}\mathcal{W}_6(t_n,S_m(t_n))-\frac{\hbar(1-\mathscr{b})t_{n-1}^{\hbar-1}}{\mathcal{P}(\mathscr{b})}\mathcal{W}_6(t_{n-1},S_m(t_{n-1}))\\
&\quad+\frac{\mathscr{b}\hbar}{\mathcal{P}(\mathscr{b})}\int_{t_n}^{t_{n-1}} \mathscr{q}^{\mathscr{b}-1}\mathcal{W}_6(\mathscr{q},S_m(\mathscr{q}))d\mathscr{q},\\
E_m(t_{n+1})&=E_m(t_0)+\frac{\hbar(1-\mathscr{b})t_n^{\hbar-1}}{\mathcal{P}(\mathscr{b})}\mathcal{W}_7(t_n,E_m(t_n))-\frac{\hbar(1-\mathscr{b})t_{n-1}^{\hbar-1}}{\mathcal{P}(\mathscr{b})}\mathcal{W}_7(t_{n-1},E_m(t_{n-1}))\\
&\quad+\frac{\mathscr{b}\hbar}{\mathcal{P}(\mathscr{b})}\int_{t_n}^{t_{n-1}} \mathscr{q}^{\mathscr{b}-1}\mathcal{W}_7(\mathscr{q},E_m(\mathscr{q}))d\mathscr{q},\\
I_m(t_{n+1})&=I_m(t_0)+\frac{\hbar(1-\mathscr{b})t_n^{\hbar-1}}{\mathcal{P}(\mathscr{b})}\mathcal{W}_8(t_n,I_m(t_n))-\frac{\hbar(1-\mathscr{b})t_{n-1}^{\hbar-1}}{\mathcal{P}(\mathscr{b})}\mathcal{W}_8(t_{n-1},I_m(t_{n-1}))\\
&\quad+\frac{\mathscr{b}\hbar}{\mathcal{P}(\mathscr{b})}\int_{t_n}^{t_{n-1}} \mathscr{q}^{\mathscr{b}-1}\mathcal{W}_8(\mathscr{q},I_m(\mathscr{q}))d\mathscr{q}.
\end{aligned}\right\}\tag{42}$$

If the function $\mathscr{q}^{\mathscr{b}-1}\mathcal{W}(\mathscr{q},\mathcal{M}(\mathscr{q}))$ is approximated over the finite interval $\left[t_i,t_{i+1}\right]$ for $i=1,2,\ldots,8$ and $\mathcal{M}=\left[S_h,E_h,I_h,T_h,R_hS_m,E_m,I_m\right]^T$, using the Lagrangian piecewise

interpolation such that

$$
\begin{aligned}
S_h(t_{n+1}) &= S_h(t_n) + \frac{\hbar(1-\mathscr{E})t_n^{\hbar-1}}{\mathcal{P}(\mathscr{E})}\mathcal{W}_1(t_n, S_h(t_n)) - \frac{\hbar(1-\mathscr{E})t_{n-1}^{\hbar-1}}{\mathcal{P}(\mathscr{E})}\mathcal{W}_1(t_{n-1}, S_h(t_{n-1})) \\
&+ \frac{\mathscr{E}\hbar}{\mathcal{P}(\mathscr{E})}\left[\frac{3}{2}(\Delta t)t_n^{\hbar-1}\mathcal{W}_1(t_n, S_h(t_n)) - \frac{1}{2}(\Delta t)t_{n-1}^{\hbar-1}\mathcal{W}_1(t_{n-1}, S_h(t_{n-1}))\right] \\
E_h(t_{n+1}) &= E_h(t_0) + \frac{\hbar(1-\mathscr{E})t_n^{\hbar-1}}{\mathcal{P}(\mathscr{E})}\mathcal{W}_2(t_n, E_h(t_n)) - \frac{\hbar(1-\mathscr{E})t_{n-1}^{\hbar-1}}{\mathcal{P}(\mathscr{E})}\mathcal{W}_2(t_{n-1}, E_h(t_{n-1})) \\
&+ \frac{\mathscr{E}\hbar}{\mathcal{P}(\mathscr{E})}\left[\frac{3}{2}(\Delta t)t_n^{\hbar-1}\mathcal{W}_2(t_n, E_h(t_n)) - \frac{1}{2}(\Delta t)t_{n-1}^{\hbar-1}\mathcal{W}_2(t_{n-1}, E_h(t_{n-1}))\right] \\
I_h(t_{n+1}) &= I_h(t_0) + \frac{\hbar(1-\mathscr{E})t_n^{\hbar-1}}{\mathcal{P}(\mathscr{E})}\mathcal{W}_3(t_n, I_h(t_n)) - \frac{\hbar(1-\mathscr{E})t_{n-1}^{\hbar-1}}{\mathcal{P}(\mathscr{E})}\mathcal{W}_3(t_{n-1}, I_h(t_{n-1})) \\
&+ \frac{\mathscr{E}\hbar}{\mathcal{P}(\mathscr{E})}\left[\frac{3}{2}(\Delta t)t_n^{\hbar-1}\mathcal{W}_3(t_n, I_h(t_n)) - \frac{1}{2}(\Delta t)t_{n-1}^{\hbar-1}\mathcal{W}_3(t_{n-1}, I_h(t_{n-1}))\right] \\
T_h(t_{n+1}) &= T_h(t_0) + \frac{\hbar(1-\mathscr{E})t_n^{\hbar-1}}{\mathcal{P}(\mathscr{E})}\mathcal{W}_4(t_n, T_h(t_n)) - \frac{\hbar(1-\mathscr{E})t_{n-1}^{\hbar-1}}{\mathcal{P}(\mathscr{E})}\mathcal{W}_4(t_{n-1}, T_h(t_{n-1})) \\
&+ \frac{\mathscr{E}\hbar}{\mathcal{P}(\mathscr{E})}\left[\frac{3}{2}(\Delta t)t_n^{\hbar-1}\mathcal{W}_4(t_n, T_h(t_n)) - \frac{1}{2}(\Delta t)t_{n-1}^{\hbar-1}\mathcal{W}_4(t_{n-1}, T_h(t_{n-1}))\right] \\
R_h(t_{n+1}) &= R_h(t_0) + \frac{\hbar(1-\mathscr{E})t_n^{\hbar-1}}{\mathcal{P}(\mathscr{E})}\mathcal{W}_5(t_n, R_h(t_n)) - \frac{\hbar(1-\mathscr{E})t_{n-1}^{\hbar-1}}{\mathcal{P}(\mathscr{E})}\mathcal{W}_5(t_{n-1}, R_h(t_{n-1})) \\
&+ \frac{\mathscr{E}\hbar}{\mathcal{P}(\mathscr{E})}\left[\frac{3}{2}(\Delta t)t_n^{\hbar-1}\mathcal{W}_5(t_n, R_h(t_n)) - \frac{1}{2}(\Delta t)t_{n-1}^{\hbar-1}\mathcal{W}_5(t_{n-1}, R_h(t_{n-1}))\right] \\
S_m(t_{n+1}) &= S_m(t_0) + \frac{\hbar(1-\mathscr{E})t_n^{\hbar-1}}{\mathcal{P}(\mathscr{E})}\mathcal{W}_6(t_n, S_m(t_n)) - \frac{\hbar(1-\mathscr{E})t_{n-1}^{\hbar-1}}{\mathcal{P}(\mathscr{E})}\mathcal{W}_6(t_{n-1}, S_m(t_{n-1})) \\
&+ \frac{\mathscr{E}\hbar}{\mathcal{P}(\mathscr{E})}\left[\frac{3}{2}(\Delta t)t_n^{\hbar-1}\mathcal{W}_6(t_n, S_m(t_n)) - \frac{1}{2}(\Delta t)t_{n-1}^{\hbar-1}\mathcal{W}_6(t_{n-1}, S_m(t_{n-1}))\right] \\
E_m(t_{n+1}) &= E_m(t_0) + \frac{\hbar(1-\mathscr{E})t_n^{\hbar-1}}{\mathcal{P}(\mathscr{E})}\mathcal{W}_7(t_n, E_m(t_n)) - \frac{\hbar(1-\mathscr{E})t_{n-1}^{\hbar-1}}{\mathcal{P}(\mathscr{E})}\mathcal{W}_7(t_{n-1}, E_m(t_{n-1})) \\
&+ \frac{\mathscr{E}\hbar}{\mathcal{P}(\mathscr{E})}\left[\frac{3}{2}(\Delta t)t_n^{\hbar-1}\mathcal{W}_7(t_n, E_m(t_n)) - \frac{1}{2}(\Delta t)t_{n-1}^{\hbar-1}\mathcal{W}_7(t_{n-1}, E_m(t_{n-1}))\right] \\
I_m(t_{n+1}) &= I_m(t_0) + \frac{\hbar(1-\mathscr{E})t_n^{\hbar-1}}{\mathcal{P}(\mathscr{E})}\mathcal{W}_8(t_n, I_m(t_n)) - \frac{\hbar(1-\mathscr{E})t_{n-1}^{\hbar-1}}{\mathcal{P}(\mathscr{E})}\mathcal{W}_8(t_{n-1}, I_m(t_{n-1})) \\
&+ \frac{\mathscr{E}\hbar}{\mathcal{P}(\mathscr{E})}\left[\frac{3}{2}(\Delta t)t_n^{\hbar-1}\mathcal{W}_8(t_n, I_m(t_n)) - \frac{1}{2}(\Delta t)t_{n-1}^{\hbar-1}\mathcal{W}_8(t_{n-1}, I_m(t_{n-1}))\right]
\end{aligned}
\tag{43}
$$

5 | Numerical Simulations

This section presents numerical simulation experiments conducted on an EC2 instance [81], based on the system model described in Equation (43). Our objective is to investigate the behavior of the mathematical model for disease spread, utilizing the scalability of cloud EC2 machines to examine the impact of fractal-fractional order derivatives and larvicidal control on malaria transmission dynamics. Figure 3 depicts the conceptual system integrations for malaria vector control.

5.1 | Simulation Design

In this experiment, we investigate the behavior of the model representing the spread of disease within a population. We used the AWS EC2 cloud Shell to run the simulation, relying on the scalability of the cloud engine resources. The focus is on examining the basic reproduction number and system dynamics under the influence of a fractal–fractional order model, as outlined in Equations (20) and (28). Our Step-by-step outline of the experimental outline involves setting up the environment as follows. First, we launched an AWS EC2 instance (c5.xlarge) on Amazon Linux 2 AMI, configuring it within a default virtual private cloud (VPC), subnet, security group, and key pair. We then connected our local machine to the EC2 instance via the SSH protocol and installed necessary dependencies, including Python and scientific libraries (e.g., NumPy, SciPy, and Matplotlib). Next, we cloned the repository containing the core simulation code, defining initial parameter values (Table 2) for the fractal fractional-order derivatives ($\mathscr{E}$ and $\hbar$). The initial conditions: $S_h(0) = 120, E_h(0) = 20, I_h(0) = 10, T_h(0) = 7, R_h(0) = 5, S_m(0) = 400, E_m(0) = 60$ and $I_m(0) = 30$. The setup numerically solves the system of differential equations governing disease spread dynamics, incorporating fractional-order derivatives. We implemented Runge–Kutta, and fractional-order Euler method to solve the system. This approach enabled us to investigate the effects of varying fractal fractional-order derivatives ($\mathscr{E}$ and $\hbar$) on system dynamics. Additionally, we examined how changes in larvicidal activity and treated mosquito nets impact the basic reproduction number.

5.2 | Result Analysis

The study derives and analyses the basic reproduction number for varying values of $\mathscr{E}$ and $\hbar$, as well as different larvicidal treatment scenarios. The results are visualized using Matplotlib, illustrating infected populations over time and the relationship between the basic reproduction number and parameter variations. The numerical outcomes are interpreted to understand the impact of fractal fractional-order derivatives and larvicidal treatment on disease dynamics. The analysis evaluates how these factors influence the basic reproduction number and overall system stability.

We realized that leveraging AWS EC2 cloud Shell offers efficient large-scale response, supporting real-time analysis and adjustments for varying parameters. This approach provided valuable insights into disease dynamics and control strategies. The basic reproduction number, denoted as R_0, was used to investigate the potential spread of an infectious disease within a population. An R_0 value below 1 suggests that each infected person causes, on average, fewer than one new infection, as shown in Figure 4. This implies that the disease will eventually diminish in the population. For instance, an R_0 of 0.2642952 indicates that each malaria-infected mosquito is expected to produce approximately 0.264 new infections in humans. According to Figure 4, when R_{0h} is 0.1962778 and R_{0m} is 0.3558831, the resulting R_0 is 0.2642952, which occurs in the context of larvicidal activity, treated mosquito nets, and effective treatment. This finding suggests that plant extracts can be employed to target mosquito larval stages, effectively reducing adult mosquito populations and, consequently, the transmission of malaria. Strong larvicidal activity can significantly decrease mosquito numbers, leading to fewer malaria cases and a lower R_0 value. Insecticide-treated nets (ITNs) create a physical barrier between humans and mosquitoes, minimizing exposure to bites, particularly at night when mosquitoes are most active. Additionally, effective treatment of infected individuals reduces the pool of infectious humans, further lowering the potential for disease transmission.

Figure 5 shows an R_0 of approximately 11.6211313 in this malaria model that includes mosquito nets and treatment but excludes larvicidal activity, such as the use of leaf extracts to reduce mosquito populations. This indicates a markedly different scenario for disease transmission. Here, R_{0h} is 35.4362504 and R_{0m} is 3.8110887. An R_0 greater than 1 implies that each infected individual, on average, causes more than one new infection, suggesting that the disease could spread and establish itself within the population. In this context, an R_0 of 11.6211313 indicates a high likelihood of malaria proliferation if no additional control measures are taken. While mosquito nets, especially insecticide-treated nets (ITNs), provide a barrier against bites, thereby reducing human exposure to malaria, they do not eliminate mosquitoes from the environment. If the mosquito population remains elevated, the risk of malaria transmission continues to be significant. Antimalarial treatment helps lessen the severity of the disease and shortens the duration of infectiousness for

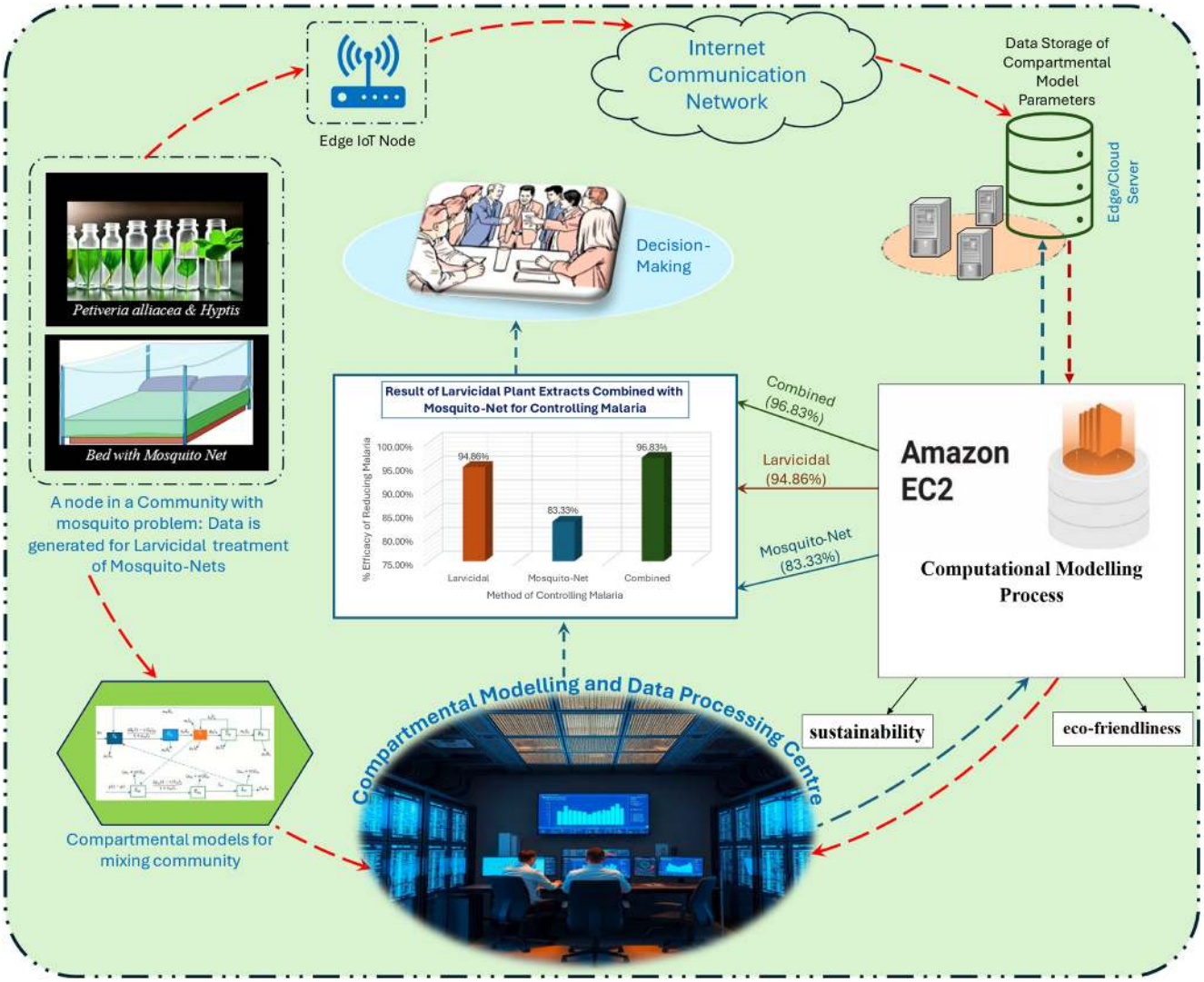


FIGURE 3 | Smart malaria control using larvicidal plant extracts and mosquito nets. With the model, sensor nodes can be installed to collect environmental data that enhance the breeding of mosquitoes and the timing of malaria-treated mosquito nets. Data collected can be processed using artificial intelligence for decision- and policy-making.

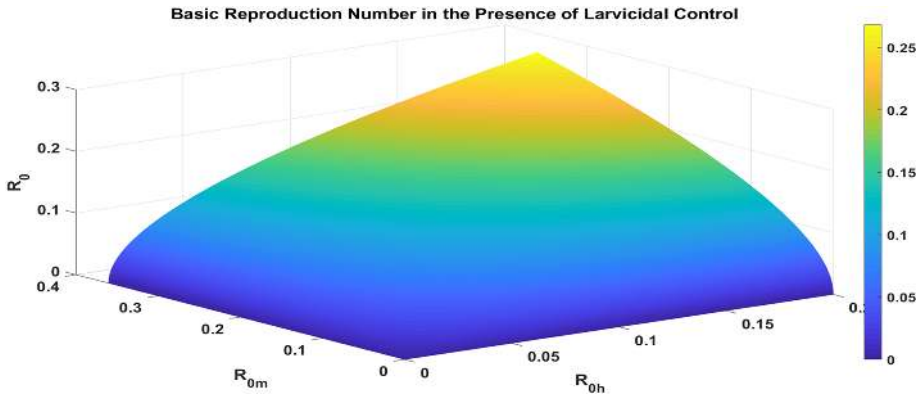


FIGURE 4 | EC2 instance numerical simulation of the basic reproduction number in the presence of larvicidal activity and other controls.

those infected. However, it does not directly impact the mosquito population, so the overall potential for transmission remains high without effective mosquito management. The larvicidal activity involves strategies to decrease mosquito populations at the larval stage, often through biological or chemical methods. Without such measures, the adult mosquito population can remain substantial, facilitating ongoing transmission. Given that many adult mosquitoes can bite humans, the likelihood of transmission

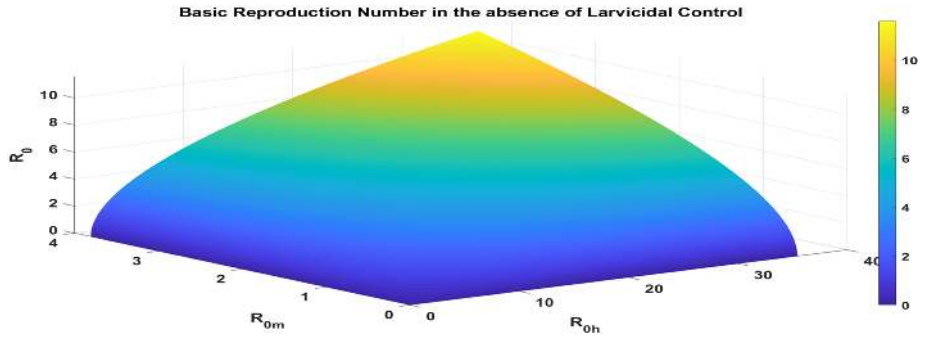


FIGURE 5 | EC2 instance numerical simulation of the basic reproduction number in the absence of larvicidal activity, while other controls are present.

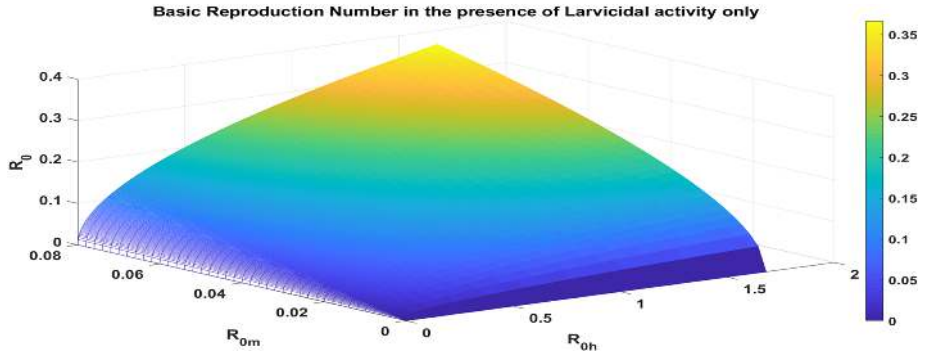


FIGURE 6 | EC2 instance numerical simulation of the basic reproduction number in the presence of larvicidal activity only.

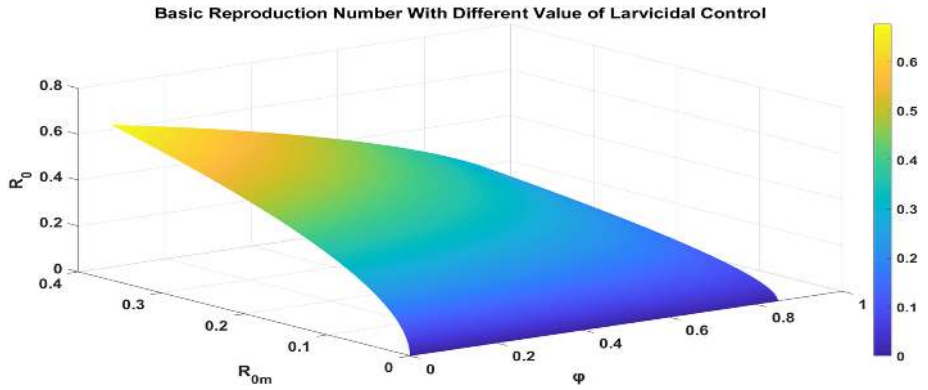


FIGURE 7 | EC2 instance numerical simulation of the basic reproduction number in the presence of larvicidal activity with values ranging from 0.1 to 0.85.

increases significantly. An R_0 of 11.6211313 suggests that the mosquito population is sufficient to sustain and even amplify malaria transmission, as the average infected mosquito could lead to over two new infections.

Figure 6 illustrates the basic reproduction number in the context of larvicidal activity, without the use of mosquito nets or treatment. The R_0 value of 0.3619049 indicates that, even in the absence of mosquito nets and treatment, larvicidal activity alone is sufficient to maintain low levels of malaria transmission. This suggests that the significant reduction in the adult mosquito population outweighs the potential increase in transmission risk from lacking nets and treatment. A low R_0 value indicates that malaria transmission is unlikely to persist under these conditions. The effective reduction of mosquitoes through larvicidal methods minimizes the likelihood of human infection. Additionally, Figure 7 demonstrates how the basic reproduction number decreases as the effectiveness of larvicidal activity increases.

Figures 8 and 9 illustrate the dynamics of mosquito and human infections using fractal fractional order derivatives, particularly concerning larvicidal activity, treated mosquito nets, and treatment. The initial increase in infected mosquitoes, as seen in Figure 8, may indicate a temporary imbalance. Even with larvicidal measures in place, some mosquitoes may survive, leading to a rise in transmission rates at first. However, as effective control measures take effect, the overall mosquito population is likely

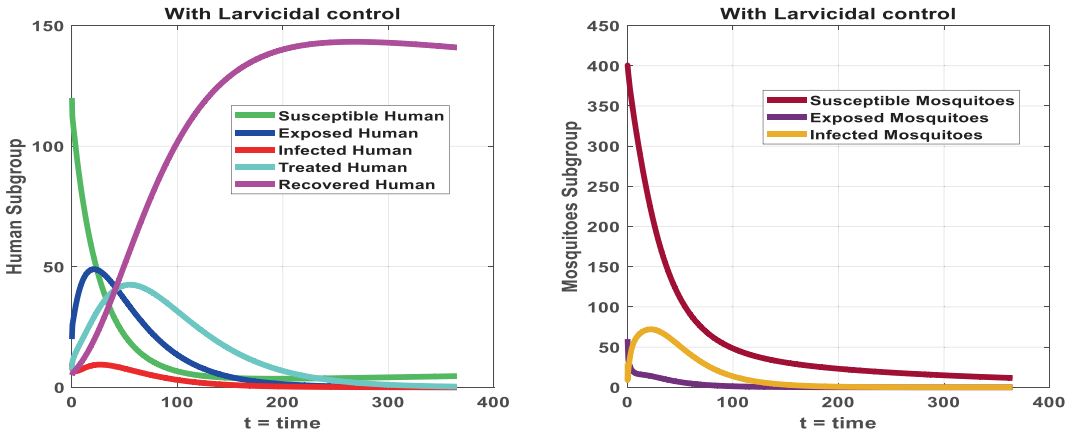


FIGURE 8 | Effect of larvicidal activity on the dynamics of the state functions for both human and mosquito subgroups on EC2 instance machines.

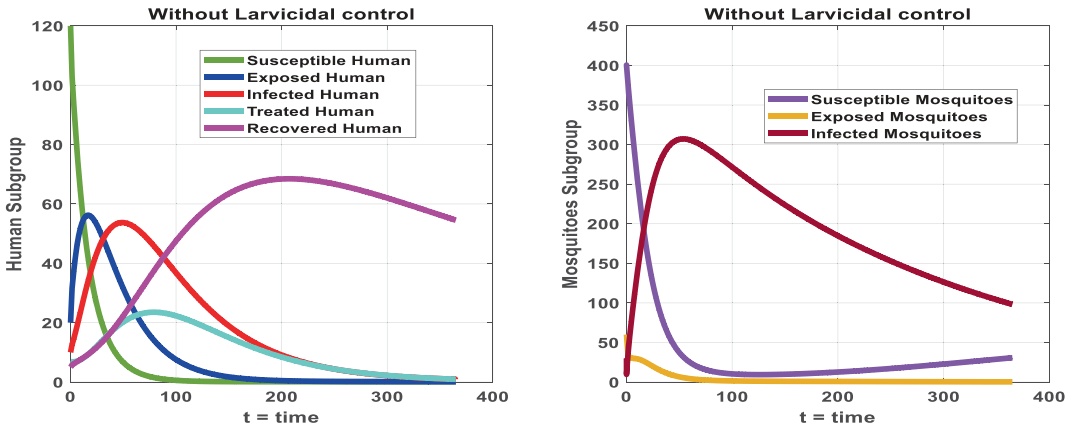


FIGURE 9 | Effect of the absence of larvicidal activity on the dynamics of the state functions for both human and mosquito subgroups on EC2 instance machines.

to begin to decline. With larvicides reducing mosquito numbers and treated nets preventing bites, the incidence of new infections in both mosquitoes and humans starts to decrease. Eventually, both populations may stabilize at lower levels, indicating a controlled environment where disease transmission is significantly reduced. In contrast, Figure 8 shows that in the absence of larvicidal activity, the mosquito population can grow unchecked, allowing infected mosquitoes to multiply without control measures. This unchecked growth results in a higher number of human infections, as transmission becomes more likely. The subsequent decline in infected mosquitoes may reflect other factors, such as natural mortality or potential immunity within the mosquito population. Initially, the infected human population may rise due to increased transmission, but will eventually decline as hosts recover or succumb to the disease. The balance between susceptible, infected, and recovered individuals in both mosquitoes and humans contributes to these observed patterns. In an infected population, once a significant number of individuals are infected, the likelihood of further transmission can decrease. The effectiveness of larvicides and treated nets is crucial in this dynamic, as they can dramatically reduce the mosquito population and lower the rate of new infections. Thus, the presence or absence of larvicidal activity and mosquito nets significantly impacts disease transmission dynamics, resulting in varying patterns in the populations of infected mosquitoes and humans.

Figure 10a–h illustrates the dynamics of different values of fractal fractional order, that is, $\mathscr{O} = \mathscr{h} = 1.00, 0.96, 0.92.\ 0.88$ and 0.84 in the presence of larvicidal activity influenced by various factors related to disease transmission, population interactions, and intervention measures over time. We observe a decreasing growth in S_h for different fractal-fractional orders: $\mathscr{O} = \mathscr{h} = 1.00, 0.96, 0.92.\ 0.88$ and 0.84. Fractional orders play significant roles, and we have obtained new results for each order. As S_h decreases, there is a sharp increase in E_h, which then immediately declines. The most significant changes in the state variables occur at the order of 1.00 within the fractal-fractional framework of derivatives.

Figure 10a–h illustrates the dynamics of the malaria transmission model. In Figure 10a, the decline in susceptible humans suggests that as the disease progresses, the pool of susceptible individuals diminishes due to infection or treatment. Effective interventions, such as larvicidal activity, further contribute to this reduction. Figure 10b reveals an initial increase in exposed humans, likely to represent individuals who are infected but not yet symptomatic (asymptomatic or pre-symptomatic). As these individuals transition to the infected state or recover, their numbers decrease, contributing to an overall reduction in human cases. The oscillations observed in the infected human population in Figure 10c reflect fluctuations in transmission dynamics,

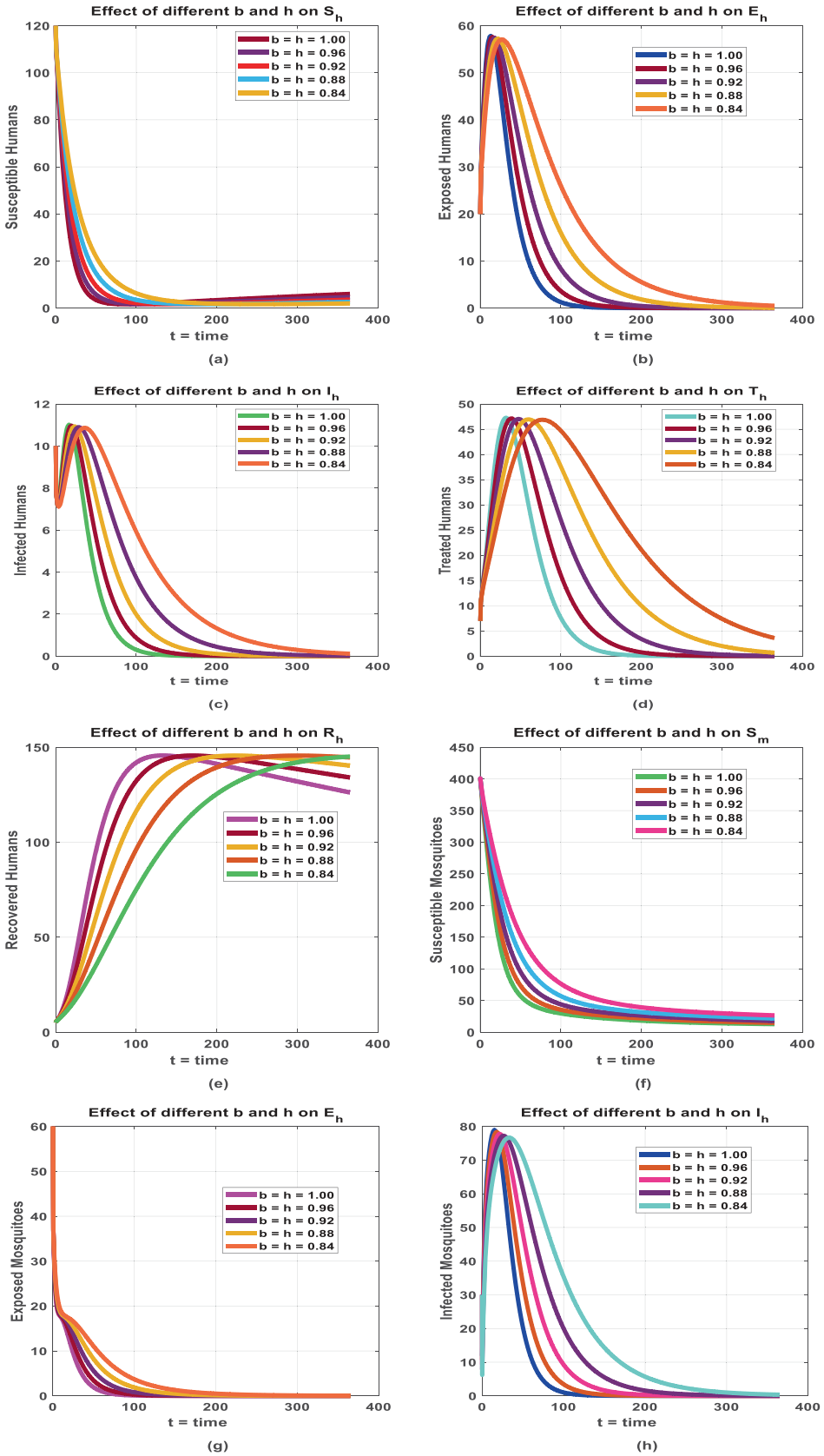


FIGURE 10 | (a, b) Effects of the fractal and fractional orders $\mathscr{b} = \mathscr{h} = 1.00, 0.96, 0.92, 0.88$ and 0.84 on the state functions S_h and E_h, respectively, on EC2 instance machines. (c, d) Effects of the fractal and fractional orders $\mathscr{b} = \mathscr{h} = 1.00, 0.96, 0.92, 0.88$ and 0.84 on the state functions I_h and T_h, respectively, on EC2 instance machines. (e, f) Effects of the fractal and fractional orders $\mathscr{b} = \mathscr{h} = 1.00, 0.96, 0.92, 0.88$ and 0.84 on the state functions R_h and S_m, respectively, on EC2 instance machines. (g, h) Effects of the fractal and fractional orders $\mathscr{b} = \mathscr{h} = 1.00, 0.96, 0.92, 0.88$ and 0.84 on the state functions E_m and I_m, respectively, on EC2 instances.

which may be influenced by varying contact rates, seasonal effects, or the impacts of interventions. Eventually, this population stabilizes as the disease is brought under control. Figure 10d shows an increase in the treated human population, indicating effective interventions that lead to an initial spike in treated individuals. The subsequent decrease and stabilization of this population reflect the natural course of recovery and the maximum treatment capacity. From Figure 10e, we note an increase in recovered humans, suggesting many individuals are recovering from the infection and contributing to a larger immune population. The stabilization of this group indicates that these individuals remain immune for a significant period. Figure 10f illustrates a decrease in susceptible mosquitoes, pointing to the success of intervention measures, such as larvicides and treated nets, which reduce the mosquito population. This directly impacts transmission dynamics by lowering the vector population. In Figure 10g, a bulge in the exposed mosquito population around 20 suggests a delay in the transition from exposed to infected states, potentially due to a period of latent infection. The eventual stabilization indicates that most of the mosquito population has either become infected or died off. The sharp increase in infected mosquitoes signifies a rapid transmission phase, occurring under conditions favorable for infection (e.g., higher mosquito and human contact). The subsequent decrease and stabilization shown in Figure 10h imply that intervention measures have effectively reduced both mosquito populations and the transmission rate. Overall, the interactions among these populations are governed by the dynamics of disease transmission, recovery, and intervention effectiveness, leading to the observed patterns as parameters change.

Figure 11a–h illustrates the population dynamics of malaria transmission, particularly concerning larvicidal control measures aimed at reducing mosquito populations to manage the disease. We observe that the population of susceptible humans is greater when larvicidal control is implemented, as it decreases more slowly compared to scenarios without such control. This may indicate that while control measures reduce mosquito populations, they also allow for a temporary increase in the human population due to reduced disease transmission, resulting in more susceptible individuals remaining. The decrease in exposed humans with the implementation of larvicidal control suggests that fewer individuals are being bitten by mosquitoes, leading to lower exposure to pathogens, an encouraging outcome of these measures. Furthermore, the significant decline in infected humans reflects the effectiveness of larvicidal control in preventing disease transmission, thereby reducing the number of new infections. The initial rise in treated humans during larvicidal control may be attributed to increased awareness and access to treatment in response to better mosquito management. However, the subsequent decline suggests that as fewer people become infected, there is less need for treatment over time. The higher number of recovered humans under larvicidal control is likely a direct result of fewer infections, contributing to a healthier population overall. The initial spike in susceptible mosquitoes may indicate that larvicidal measures initially affect older, infected populations, while younger, susceptible mosquitoes continue to emerge. Over time, as larvicidal measures effectively reduce the overall mosquito population, the number of susceptible mosquitoes eventually declines. The decrease in exposed mosquitoes in the presence of larvicidal measures suggests that these interventions may be impacting population dynamics in a way that does not allow mosquitoes to engage with hosts or reproduce, potentially due to the complete coverage or efficacy of the larvicides. In contrast, the significantly higher population of infected mosquitoes when no larvicides are used reflects a direct relationship between mosquito population size and the rate of transmission. Without control measures, more mosquitoes can be produced and feed on infected hosts, resulting in a higher infection rate.

These observations illustrate the complex interplay between vector control, disease transmission, and population dynamics. Effective larvicidal measures can significantly reduce infection rates in both humans and mosquitoes, thereby altering the balance of susceptible, exposed, infected, treated, and recovered populations over time.

Table 3 presents a comparative analysis of the efficacy of three malaria control methods: larvicidal control, mosquito nets, and a combination of both. The numerical values represent the effectiveness of each method in reducing mosquito populations and controlling malaria infections. For instance, larvicidal control achieves a high efficacy of 94.86%, significantly reducing the presence of malaria-causing agents. Mosquito net control is 83.33% effective, while the combination of both methods yields the highest efficacy of 96.83%. This suggests that integrating larvicidal control with mosquito nets provides the most effective protection against malaria. The key observations from our analysis include:

- Larvicidal control alone is highly effective (94.86%), outperforming mosquito net control alone (83.33%).
- The combination of larvicidal control and mosquito nets yields the highest efficacy (96.83%), indicating that an integrated approach is more beneficial for public health interventions.
- The proposed larvicidal model demonstrates its potential as a robust tool for malaria prevention strategies and can be prioritized or combined with other measures for maximum impact.

Therefore, public health programs targeting malaria could greatly benefit from emphasizing larvicidal control, either as a standalone intervention or in combination with mosquito nets for enhanced results.

This study used the fractal-fractional derivative model (FFM) for larvicidal control of malaria. This extends classical and fractional-order models by incorporating memory effects and environmental heterogeneity. Below provides a comparison of the findings with previous approaches. Traditional malaria larvicidal control models (e.g., deterministic compartmental models) often use integer-order differential equations to describe larval and adult mosquito population dynamics. These models typically assume instantaneous interactions and constant environmental conditions. However, human populations residing in temperate regions of the real world exhibit long-term memory effects and varying environmental factors, which cannot be studied using integer-order. The proposed FFM, formulated with the Caputo Fabrizio derivative, accounts for these complexities. Compared to classical models:

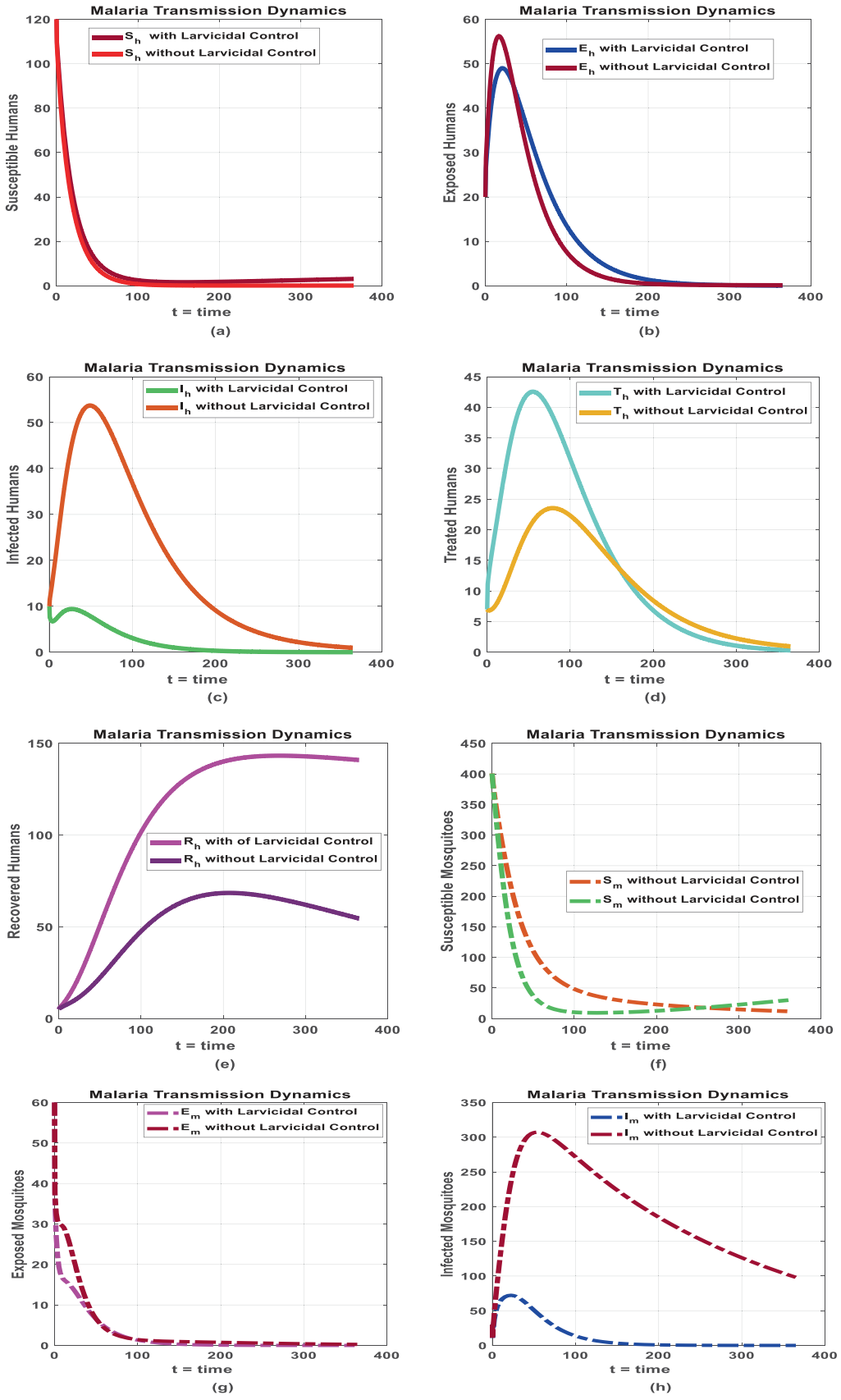


FIGURE 11 | (a, b) Dynamics of susceptible and exposed humans in the presence and absence of larvicidal activity on EC2 instance machines. (c, d) Dynamics of infected and treated humans in the presence and absence of larvicidal activity. (e, f) Dynamics of recovered humans and susceptible mosquitoes in the presence and absence of larvicidal activity on EC2 instance machines. (g, h) Dynamics of exposed and infected mosquitoes in the presence and absence of larvicidal activity on EC2 instance machines.

TABLE 3 | Comparison of different controls (larvicidal, mosquito net, and both).

Model type	Larvicidal	Mosquito net	Both
Efficacy of control	20.55	66.66	12.69
% Efficacy	94.86%	83.33%	96.83%

- Our proposed approach captures the non-local interactions in mosquito dynamics better than integer-order models.
- The inclusion of fractional memory terms results in a more accurate prediction of larvicidal suppression over time under different larvicidal application scenarios.
- The fractal component reflects spatial heterogeneity, improving ecological realism.

Existing FFMs for malaria control (e.g., Caputo or Riemann-Liouville derivatives) incorporate memory effects but do not consider fractal structures in mosquito breeding sites. These models demonstrate improved accuracy over classical models but still assume uniform environmental conditions. To further validate our model, we conducted numerical simulations comparing our results with existing methods (e.g., classical Runge–Kutta solutions as in [82]). Figures 8–10 illustrate the enhanced performance of our model in capturing the long-term effects of larvicidal intervention. To enhance our results, Internet of Things (IoT) vector sensors, such as IoT-networked robots [83], and Agentic Artificial Intelligence [84], can be tested for optimization of larvicides in Figure 4.

With the FFM designed to show how plant-based larvicides affect mosquito density, the Agentic algorithm forms the next logical stage of our work. Through IoT, real-world data such as mosquito density, larvicide application rates, and environmental variables can be ingested via IoT middleware [85]. These IoT sensors monitor mosquito breeding domains (e.g., larva presence, pH, temperature, and humidity). Similar to the approach in [86], the Agentic algorithm maps IoT data into the FFM computational model as the input layer, learning and updating predictions dynamically (e.g., when and where to apply larvicides), while generating disease risk maps and predicting interventions (adjusting strategies based on resistance trends or weather conditions). This forms the Agentic model layer. Finally, the core Agentic layer autonomously interprets the model output of Figure 2, mapping high-risk zones for prioritization and profiling targeted larvicide deployments. The Agentic AI output also extends coordination with other smart systems, such as wearables, alert notices, spraying drones, surveillance, and community outreach.

5.3 | Policy Implications and Future Technology Focus

This paper has identified the five main policy interventions for future Agentic AI integration.

- Governments and public health institutions should consider promoting and scaling up the use of eco-friendly larvicides derived from plant extracts in malaria-endemic regions.
- Integrated vector management programs should focus on combining interventions to achieve synergistic effects in reducing malaria transmission. In context, leveraging IoT and Agentic AI can be explored to facilitate real-time monitoring and enable early warning interventions in Figure 2.
- Continuous investment in the use of computational modeling to optimize strategies for controlling vector-borne diseases.
- Promoting the use of biological larvicides to reduce reliance on chemical insecticides, thereby reducing costs, health problems to hosts, and supporting sustainable public health infrastructure [87]. Such public smart health infrastructure should fully adopt Agentic cloud surveillance analytics to enhance decision-making efficiency.

6 | Conclusion

This study presents an integrated compartmental model to control mosquito and malaria spread using larvicidal plant extracts. Two population groups (human and mosquito) are considered, and two larvicidal plant extracts (*Petiveria Alliacea* and *Hyptis Suavolens*) are studied. The fractal-fractional order compartmental model uses its memory effect property to evaluate the susceptibility of infected, treated, and recovered people from malaria. With its non-local properties, the proposed model investigates larger dynamics than the integer and fractional order models. The model evaluates heterogeneous breeding and survival domains of the disease-bearing mosquitoes—the adult female Anopheles. Over an AWS EC2-accelerated computational platform used in the study, our proposed model reveals that larvicidal control achieves a high efficacy of 94.86%, outperforming mosquito net control alone (83.33%). Additional results show that combining larvicidal control with mosquito nets yields the highest efficacy of 96.83%. These results underscore the value of integrated strategies for malaria management and highlight the potential of larvicidal plant extracts as a vital addition to existing control measures. The study has important implications for public health, particularly in resource-limited settings. By targeting mosquito larvae, these extracts reduce the adult mosquito population and thereby limit malaria transmissions and deaths. As global malaria elimination efforts advance, our findings offer critical insights into the development of effective, sustainable, and integrated vector control strategies. We also showed that sensors and the internet of things infrastructure can be installed to enhance the understanding and control of the malaria disease vector. Future efforts should explore the use of Agentic AI and Internet of Things real-time monitoring to enhance malaria control.

Author Contributions

Juliet Onyinye Nwigwe: conceptualization, writing – original draft, writing – review and editing, methodology. **Kennedy Chinedu Okafor:** writing – review and editing, methodology, software, validation, formal analysis, project administration, funding acquisition. **Ogonna Christiana Ani:** writing – original draft, conceptualization, writing – review and editing, software, data curation, visualization. **Titus Ifeanyi Chinebu:** conceptualization, methodology, software, validation, formal analysis, writing – original draft, data curation. **Okafor Ijeoma Peace:** formal analysis, writing – review and editing, investigation,

validation. **Omowunmi Mary Longe:** writing – original draft, investigation, validation, formal analysis, supervision, funding acquisition. **Kelvin Anoh:** conceptualization, methodology, software, formal analysis, supervision, project administration.

Acknowledgments

We extend our appreciation to the Institute of Electrical and Electronics Engineers (IEEE), USA, for their generous grant support under the project titled "*Automated Borehole Design and Massive Rural Health Education in Iji-Nike Community in Enugu State (22-HAC-119)*." Their contribution was instrumental in the successful implementation of the automated borehole system, which has significantly alleviated water scarcity in the Iji-Nike community. We also acknowledge the local community for their cooperation and support throughout the project phases. Special thanks go to the research team for their dedication and innovative work on the mathematical model for malaria dynamics, which has paved the way for sustainable and eco-friendly malaria control measures. This project would not have been possible without the collaborative efforts and commitment of all stakeholders involved.

Conflicts of Interest

The authors declare no conflicts of interest.

Data Availability Statement

The data that support the findings of this study are available on request from the corresponding author. The data are not publicly available due to privacy or ethical restrictions.

References

1. World Health Organization, *African Health Ministers Commit to End Malaria Deaths* (World Health Organization, 2024), https://www.who.int/news/item/06-03-2024-african-health-ministers-commit-to-end-malaria-deaths.

2. World Health Organization, *World Malaria Day 2024: Accelerating the Fight Against Malaria for a More Equitable World* (World Health Organization, 2024), https://www.who.int/news/item/24-04-2024-world-malaria-day-2024-accelerating-the-fight-against-malaria-for-a-more-equitable-world.

3. World Health Organization, 2024, https://www.who.int/news-room/fact-sheets/details/Vector-bornediseases.

4. University of Pretoria, "Malaria Frequently Asked Questions," 2024, https://www.up.ac.za/up-institute-for-sustainable-malaria-control/article/2243486/malaria-frequently-asked-questions.

5. J. Mohammed-Awel and B. G. Abba, "Mathematics of an Epidemiology-Genetics Model for Assessing the Role of Insecticides Resistance on Malaria Transmission Dynamics," *Mathematical Biosciences* 312 (2019): 33–49.

6. WHO, "Malaria: Draft Global Technical Strategy," Sixty-Eighth World Health Assembly, 2015.

7. WHO, "World Malaria Report," 2017.

8. D. K. W. Blayneh and J. Mohammed-Awel, "Insecticide-Resistant Mosquitoes and Malaria Control," *Mathematical Biosciences* 252 (2014): 14–26.

9. D. Bourguet, A. Genissel, and M. Raymond, "Insecticide Resistance and Dominance Levels," *Journal of Economic Entomology* 93 (2000): 1588–1595.

10. Z. S. Brown, K. L. Dickinson, and R. A. Kramer, "Insecticide Resistance and Malaria Vector Control: The Importance of Fitness Cost Mechanisms in Determining Economically Optimal Control Trajectories," *Journal of Economic Entomology* 106 (2013): 366–374.

11. L. Cai, M. Martcheva, and X. Li, "Epidemic Models With Age of Infection, Indirect Transmission and Incomplete Treatment," *Discrete and Continuous Dynamical Systems* 18 (2013): 2239–2265.

12. N. Chitnis, J. M. Hyman, and J. M. Cushing, "Determining Important Parameters in the Spread of Malaria Through the Sensitivity Analysis of a Mathematical Model," *Bulletin of Mathematical Biology* 70 (2008): 1272–1296.

13. https://www.cdc.gov/malaria/about/disease.html.

14. A. Prabowo, *Malaria: Mencegah Dan Mengatasi* (Niaga Swadaya, 2004).

15. C. A. B. Braganza and A. M. D. Mendoza, "The Development of a Larvicidal Tablet Using Saba Banana (*Musa acuminata* × Balbisiana) Peel Extract," in *2019 IEEE Integrated STEM Education Conference (ISEC), Princeton, NJ, USA* (IEEE, 2019), 15–17, https://doi.org/10.1109/ISECon.2019.8882035.

16. T. K. Milugo, D. P. Tchouassi, R. A. Kavishe, R. R. Dinglasan, and B. Torto, "Naturally Occurring Compounds With Larvicidal Activity Against Malaria Mosquitoes," *Frontiers in Tropical Diseases* 2 (2021): 718804, https://doi.org/10.3389/fitd.2021.718804.

17. G. F. Killeen, A. Seyoum, and B. G. J. Knols, "Rationalizing Historical Successes of Malaria Control in Africa in Terms of Mosquito Resource Availability Management," *American Journal of Tropical Medicine and Hygiene* 71 (2004): 87–93.

18. WHO, *Larval Source Management—A Supplementary Measure for Malaria Vector Control. An Operational Manual* (World Health Organization, 2013).

19. WHO, *Guidelines for Malaria Vector Control* (World Health Organization, 2019).

20. A. Bouba, K. B. Helle, and K. A. Schneider, "Predicting the Combined Effects of Case Isolation, Safe Funeral Practices, and Contact Tracing During Ebola Virus Disease Outbreaks," *PLoS One* 18, no. 1 (2023): e0276351.

21. F. Brauer, "Mathematical Epidemiology: Past, Present, and Future," *Infectious Disease Modelling* 2, no. 2 (2017): 113–127.

22. S. Zhao and H. Chen, "Modeling the Epidemic Dynamics and Control of COVID-19 Outbreak in China," *Quantitative Biology* 8 (2020): 11–19.

23. O. J. Peter, A. A. Ayoade, A. I. Abioye, A. A. Victor, and C. E. Akpan, "Sensitivity Analysis of the Parameters of a Cholera Model," *Journal of Applied Sciences and Environmental Management* 22, no. 4 (2018): 477–481.

24. W. A. Iddrisu, I. Iddrisu, and A.-K. Iddrisu, "Modeling Cholera Epidemiology Using Stochastic Differential Equations," *Journal of Applied Mathematics* 2023 (2023): 1–17.

25. J. Agbomola and A. Loyinmi, "A Mathematical Model for the Dynamical Behavior of Ebola Virus Transmission in Human-Bat Population: Implication of Immediate Discharge of Recovered Individuals," 2022.

26. I. Ahmed, G. U. Modu, A. Yusuf, P. Kumam, and I. Yusuf, "A Mathematical Model of Coronavirus Disease (COVID-19) Containing Asymptomatic and Symptomatic Classes," *Results in Physics* 21 (2021): 103776.

27. T. Berge, J. M.-S. Lubuma, G. M. Moremedi, N. Morris, and R. Kondera-Shava, "A Simple Mathematical Model for Ebola in Africa," *Journal of Biological Dynamics* 11, no. 1 (2017): 42–74.

28. M. Ali, A. L. Lopez, Y. A. You, et al., "The Global Burden of Cholera," *Bulletin of the World Health Organization* 90, no. 3 (2012): 209–218.

29. O. C. Collins and K. J. Duffy, "Estimating the Impact of Lock-Down, Quarantine and Sensitization in a COVID-19 Outbreak: Lessons From the COVID-19 Outbreak in China," *PeerJ* 8 (2020): e9933.

30. O. C. Collins and K. J. Duffy, "Mathematical Analyses on the Effects of Control Measures for a Waterborne Disease Model With Socioeconomic Conditions," *Journal of Computational Biology* 28, no. 1 (2021): 19–32.

31. O. C. Collins and K. S. Govinder, "Incorporating Heterogeneity Into the Transmission Dynamics of a Waterborne Disease Model," *Journal of Theoretical Biology* 356 (2014): 133–143.

32. F. F. Herdicho, W. Chukwu, and H. Tasman, "An Optimal Control of Malaria Transmission Model With Mosquito Seasonal Factor," *Results in Physics* 25 (2021): 104238.

33. M. A. Ibrahim and A. Denes, "A Mathematical Model for Lassa Fever Transmission Dynamics in a Seasonal Environment With a View to the 2017 e20 Epidemic in Nigeria," *Nonlinear Analysis: Real World Applications* 60 (2021): 103310.

34. M. M. Ojo, B. Gbadamosi, T. O. Benson, O. Adebimpe, and A. L. Georgina, "Modeling the Dynamics of Lassa Fever in Nigeria," *Journal of the Egyptian Mathematical Society* 29, no. 1 (2021): 1–19.

35. J. C. Koella and R. Antia, "Epidemiological Models for the Spread of Anti-Malarial Resistance," *Malaria Journal* 2, no. 1 (2003): 1–11.

36. S. Kim, J. H. Byun, A. Park, and I. H. Jung, "A Mathematical Model for Assessing the Effectiveness of Controlling Relapse in Plasmodium Vivax Malaria Endemic in the Republic of Korea," *PLoS One* 15, no. 1 (2020): e0227919.

37. J. H. Tien and D. J. Earn, "Multiple Transmission Pathways and Disease Dynamics in a Waterborne Pathogen Model," *Bulletin of Mathematical Biology* 72, no. 6 (2010): 1506–1533.

38. J. Tumwiine, S. D. Hove-Musekwa, and F. Nyabadza, "A Mathematical Model for the Transmission and Spread of Drug Sensitive and Drug-Resistant Malaria Strains Within a Human Population," *International Scholarly Research Notices* 2014 (2014): 1–12.

39. A. L. Mojeeb, C. Yang, and I. K. Adu, "Mathematical Model of Malaria Transmission With Optimal Control in The Democratic Republic of the Congo," *Journal of Mathematical and Statistical Analysis* 2 (2019): 1–14.

40. Z. Zhao, S. Li, and Y. Lu, "Mathematical Models for the Transmission of Malaria With Seasonality and Ivermectin," *Electronic Journal of Differential Equations* 28 (2022): 1–22.

41. L. J. White, R. J. Maude, W. Pongtavornpinyo, et al., "The Role of Simple Mathematical Models in Malaria Elimination Strategy Design," *Malaria Journal* 8, no. 1 (2009): 212–310.

42. B. Modu, N. Polovina, and S. Konur, "Agent-Based Modeling of Malaria Transmission," *IEEE Access* 11 (2023): 19794–19808, https://doi.org/10.1109/ACCESS.2023.3248292.

43. M. Farman, N. Gokbulut, U. Hurdoganoglu, E. Hincal, and K. Suer, "Fractional Order Model of MRSA Bacterial Infection With Real Data Fitting: Computational Analysis and Modeling," *Computers in Biology and Medicine* 173 (2024): 108367, https://doi.org/10.1016/j.compbiomed.2024.108367.

44. M. Farman, K. Jamil, C. Xu, K. S. Nisar, and A. Amjad, "Fractional Order Forestry Resource Conservation Model Featuring Chaos Control and Simulations for Toxin Activity and Human-Caused Fire Through Modified ABC Operator," *Mathematics and Computers in Simulation* 227 (2025): 282–302, https://doi.org/10.1016/j.matcom.2024.07.038.

45. A. Atangana and S. Qureshi, "Modeling Attractors of Chaotic Dynamical Systems With Fractal Fractional Operators," *Chaos, Solitons and Fractals* 123 (2019): 320–337.

46. L. Zhongfei, L. Zhuang, and M. A. Khan, "Fractional Investigation of Bank Data With Fractal Fractional Caputo Derivative," *Chaos, Solitons & Fractals* 131 (2020): 1–12.

47. S. Jain, "Numerical Analysis for the Fractional Diffusion and Fractional Buckmaster's Equation by the Step Adam-Bashforth Method," *European Physical Journal Plus* 133, no. 19 (2018): 1–11, https://doi.org/10.1140/epjp/i2018-11854-x.

48. A. Atangana and S. Jain, "A New Numerical Approximation of the Fractal Ordinary Differential Equation," *European Physical Journal Plus* 133, no. 37 (2018): 1–15.

49. A. Atangana and S. Jain, "Models of Fluid Owing in Non-Conventional Media: New Numerical Analysis," *Discrete and Continuous Dynamical Systems — Series S* 13, no. 3 (2020): 467–484.

50. A. A. Akgül, "Novel Method for a Fractional Derivative With Non-Local and Nonsingular Kernel," *Chaos, Solitons & Fractals* 114 (2018): 478–482.

51. K. Owolabi, A. Atangana, and A. Akgül, "Modeling and Analysis of Fractal Fractional Partial Differential Equations: Application to Reaction-Diffusion Model," *Alexandria Engineering Journal* 59 (2020): 2477–2490.

52. A. Atangana, A. Akgül, and K. Owolabi, "Analysis of Fractal Fractional Differential Equations," *Alexandria Engineering Journal* 59 (2020): 1117–1134.

53. A. Atangana, "Fractal-Fractional Differentiation and Integration: Connecting Fractal Calculus and Fractional Calculus to Predict Complex Systems," *Chaos, Solitons & Fractals* 102 (2017): 396–406, https://doi.org/10.1016/j.chaos.2017.04.027.

54. M. Farman, A. Shehzad, K. S. Nisar, E. Hincal, and A. Akgul, "A Mathematical Fractal-Fractional Model to Control Tuberculosis Prevalence With Sensitivity, Stability, and Simulation Under Feasible Circumstances," *Computers in Biology and Medicine* 178 (2024): 108756, https://doi.org/10.1016/j.compbiomed.2024.108756.

55. M. Farman, A. Akgül, M. Sultan, et al., "Numerical Study and Dynamics Analysis of Diabetes Mellitus With Co-Infection of COVID-19 Virus by Using Fractal Fractional Operator Scientific Reports," *Nature* 14 (2024): 16489, https://doi.org/10.1038/s41598-024-60168-6.

56. J. F. Gomez-Aguilar, T. Cordova-Fraga, T. Abdeljawad, A. Khan, and H. Khan, "Analysis of Fractal-Fractional Malaria Transmission Model," *Fractals* 28 (2020): 2040041, https://doi.org/10.1142/S0218348X20400411.

57. N. R. Chitnis, "Using Mathematical Models in Controlling the Spread of Malaria" (PhD thesis, University of Arizona, Tucson, AZ, USA, 2005).

58. B. Traoré, B. Sangare, and S. Traore, "A Mathematical Model of Malaria Transmission With Structured Vector Population and Seasonality," *Journal of Applied Mathematics* 2017 (2017): 6754097.

59. M. Osman, I. Adu, and A. K. Isaac, "Simple Mathematical Model for Malaria Transmission," *Journal of Advances in Mathematics and Computer Science* 25, no. 6 (2017): 1–24.

60. D. Agnes, "A Mathematical Model for Effective Control and Possible Eradication of Malaria" (PhD thesis, University of Cape Coast, Cape Coast, Ghana, 2020).

61. S. Olaniyi and O. S. Obabiyi, "Mathematical Model for Malaria Transmission Dynamics in Human and Mosquito Populations With Nonlinear Forces of Infection," *International Journal of Pure and Applied Mathematics* 88, no. 1 (2013): 125–156, https://doi.org/10.12732/ijpam.v88i1.10.

62. A. A. Bobbo, M. S. Pukuma, and M. A. Qadeer, "Assessment of Larvicidal Activity of Hyptis Suaveolens and *Balanites aegyptiaca* Leaves and Root Extracts Against Mosquito Species," *International Journal of Scientific and Research Publications* 6, no. 3 (2016): 10.

63. J. I. Abok, A. Ombugadu, and G. A. Angbalaga, "*Hyptis suaveolens* Extract Exhibits Larvicidal Activity Against *Anopheles gambiae* Larvae," *Journal of Natural Products Research* 2, no. 5 (2018): 245–249.

64. O. E. Ayodeji, "Biopesticidal Activities of Three Botanicals (*Ageratum conyzoides* L., Petiveria Alliacea L. and *Hyptis suaveolens* L. Poit,) Against *Sitophilus oryzae* L.," *Open Access Journal of Science* 6, no. 1 (2023): 61–66, https://doi.org/10.15406/oajs.2023.06.00194.

65. M. Muhammed, S. Dugassa, M. Belina, S. Zohdy, S. R. Irish, and A. Gebresilassie, "Insecticidal Efects of Some Selected Plant Extracts Against Anopheles Stephensi (Culicidae: Diptera)," *Malaria Journal* 21 (2022): 295, https://doi.org/10.1186/s12936-022-04320-5.

66. A. Yagoo, M. C. J. Milton, J. Vilvest, I. Johnson, and K. Balakrishna, "Mosquito Larvicidal, Pupicidal and Ovidical Effects of the Different Extracts of the Leaves of *Peltophorum pterocarpum* Against Aedes Aegypti and *Culex quinquefasciatus*," *Future Journal of Pharmaceutical Sciences* 9 (2023): 32, https://doi.org/10.1186/s43094-023-00483-3.

67. E. A. Levashina, A. Kuehn, K. Matuschewski, and Y. Schlein, "Mosquito Microevolution Drives *Plasmodium falciparum* Dynamics," *Nature Microbiology* 4, no. 8 (2019): 1303–1312, https://doi.org/10.1038/s41564-019-0452-1.

68. G. K. Christophides, B. Agianian, Z. Yang, and F. C. Kafatos, "Understanding How Mosquitoes Fight Malaria," *Science* 323, no. 5910 (2009): 1488–1493, https://doi.org/10.1126/science.1167659.

69. World Health Organization, 2023, https://www.who.int/news-room/fact-sheets/details/Malaria.

70. C. N. Ngonghala, S. Y. Del Valle, R. Zhao, and J. Mohammed-Awel, "Quantifying the Impact of Decay in Bed-Net Efficacy on Malaria Transmission," *Journal of Theoretical Biology* 363 (2014): 247–261.

71. G. Edwards and G. A. Biagini, "Resisting Resistance: Dealing With the Irrepressible Problem of Malaria," *British Journal of Clinical Pharmacology* 61, no. 6 (2006): 690–693.

72. S. I. Oke, M. M. Ojo, M. O. Adeniyi, and M. B. Matadi, "Mathematical Modeling of Malaria Disease With Control Strategy," *Communications in Mathematical Biology and Neuroscience* 2020 (2020): 43, https://doi.org/10.28919/cmbn/4513.

73. T. D. Keno, L. B. Dano, and G. A. Ganati, "Optimal Control and Cost-Effectiveness Strategies of Malaria Transmission With Impact of Climate Variability," *Journal of Mathematics* 2022 (2022): 5924549.

74. M. A. E. Noutcha and C. I. Anumudu, "*Anopheles gambiae* Complex: Molecular Forms and Occurrence of KDR Gene in Rural Southwestern Nigeria," *Nigerian Journal of Entomology* 28 (2011): 7–16.

75. Y. Dong, S. Das, C. Cirimotich, J. A. Souza-Neto, K. J. McLean, and G. Dimopoulos, "Engineered Anopheles Immunity to Plasmodium Infection," *PLoS Pathogens* 7, no. 12 (2011): 12, https://doi.org/10.1371/journal.ppat.1002458.

76. K. M. Owolabi and A. Shikongo, "Fractal Fractional Operator Method on her2+ Breast Cancer Dynamics," *International Journal of Applied and Computational Mathematics* 7, no. 3 (2021): 85.

77. A. Atangana and A. Shafiq, "Differential and Integral Operators With Constant Fractional Order and Variable Fractional Dimension," *Chaos, Solitons and Fractals* 127 (2019): 226–243.

78. A. Atangana, "Fractal-Fractional Differentiation and Integration: Connecting Fractal Calculus and Fractional Calculus to Predict Complex System," *Chaos, Solitons and Fractals* 102 (2017): 396–406.

79. M. Farman, A. Shehzad, A. Akgül, E. Hincal, D. Baleanu, and S. M. el Din, "A Fractal-Fractional Sex Structured Syphilis Model With Three Stages of Infection and Loss of Immunity With Analysis and Modeling," *Results in Physics* 54 (2023): 107098.

80. M. Farman, M. Amin, A. Akgül, A. Ahmad, M. B. Riaz, and S. Ahmad, "Fractal-Fractional Operator for COVID-19 (Omicron) Variant Outbreak With Analysis and Modeling," *Results in Physics* 39 (2022): 105630.

81. A. H. D. Mendes, M. J. F. Rosa, M. A. Marotta, A. Araujo, A. C. M. A. Melo, and C. G. Ralha, "MAS-Cloud+: A Novel Multi-Agent Architecture With Reasoning Models for Resource Management in Multiple Providers," *Future Generation Computer Systems* 154 (2024): 16–34, https://doi.org/10.1016/j.future.2023.12.022.

82. T. I. Chinebu, E. O. Ezennorom, and J. U. Okwor, "Simulation of a Mathematical Model of Malaria Transmission Dynamics in the Presence of Mosquito Net, Fumigation and Treatment," *International Journal of Trend in Scientific Research and Development (IJTSRD)* 2 (2018): 6.

83. K. C. Okafor, K. Anoh, T. I. Chinebu, B. Adebisi, and G. A. Chukwudebe, "Mitigating COVID-19 Spread in Closed Populations Using Networked Robots and Internet of Things," *IEEE Internet of Things Journal* 11, no. 24 (2024): 39424–39434, https://doi.org/10.1109/JIOT.2024.3431874.

84. D. B. Acharya, K. Kuppan, and B. Divya, "Agentic AI: Autonomous Intelligence for Complex Goals—A Comprehensive Survey," *IEEE Access* 13 (2025): 18912–18936, https://doi.org/10.1109/ACCESS.2025.3532853.

85. Z. Zeng, C. Xie, W. Tao, Y. Zhu, and H. Cai, "Knowledge-Graph-Based IoTs Entity Discovery Middleware for Nonsmart Sensor," *IEEE Transactions on Industrial Informatics* 20, no. 2 (2024): 2551–2563, https://doi.org/10.1109/TII.2023.3292540.

86. H. Zhang, T. Lyu, H. Li, et al., "AgentMario: A Multitask Agent for Robotic Interaction With Locker Systems," *IEEE Internet of Things Journal* 12, no. 3 (2025): 2473–2485, https://doi.org/10.1109/JIOT.2024.3470835.

87. T. I. Chinebu, K. C. Okafor, K. Anoh, et al., "Smart Waterborne Disease Control for a Scalable Population Using Biodynamic Model in IoT Network," *Computers in Biology and Medicine* 181 (2024): 109034, https://doi.org/10.1016/j.compbiomed.2024.109034.

Appendix A

Expansion of the Characteristic Equation of $J(E_0^*)$ of (1) at E_0, That Is, Equation (A1)

$$
\begin{aligned}
&\lambda^5 + \left[(\mu_h+\gamma_h)+(\mu_h+\phi_h+\sigma_h)+(\mu_h+\varepsilon_h+\pi_h)+(\mu_h+\omega_h)\right.\\
&\left.+(\mu_m+\xi_m+\eta\tau)\right]\lambda^4 + \left[(\mu_h+\gamma_h)(\mu_h+\phi_h+\sigma_h)+(\mu_h+\gamma_h)\right.\\
&\times(\mu_h+\varepsilon_h+\pi_h)+(\mu_h+\gamma_h)(\mu_m+\xi_m+\eta\tau)+(\mu_h+\gamma_h)(\mu_m+\eta\tau+\sigma_m)\\
&+(\mu_h+\phi_h+\sigma_h)(\mu_h+\varepsilon_h+\pi_h)+(\mu_h+\phi_h+\sigma_h)(\mu_m+\xi_m+\eta\tau)\\
&+(\mu_h+\phi_h+\sigma_h)(\mu_m+\eta\tau+\sigma_m)+(\mu_h+\varepsilon_h+\pi_h)(\mu_m+\xi_m+\eta\tau)\\
&+(\mu_h+\varepsilon_h+\pi_h)(\mu_m+\eta\tau+\sigma_m)+(\mu_m+\xi_m+\eta\tau)(\mu_m+\eta\tau+\sigma_m)\\
&\left.-\phi_h\varepsilon_h\right]\lambda^3 + \left[(\mu_h+\gamma_h)(\mu_h+\phi_h+\sigma_h)(\mu_h+\varepsilon_h+\pi_h)+(\mu_h+\gamma_h)\right.\\
&\times(\mu_h+\phi_h+\sigma_h)(\mu_m+\xi_m+\eta\tau)+(\mu_h+\gamma_h)(\mu_h+\phi_h+\sigma_h)\\
&\times(\mu_m+\eta\tau+\sigma_m)+(\mu_h+\gamma_h)(\mu_h+\varepsilon_h+\pi_h)(\mu_m+\xi_m+\eta\tau)+(\mu_h+\gamma_h)\\
&\times(\mu_h+\varepsilon_h+\pi_h)(\mu_m+\eta\tau+\sigma_m)+(\mu_h+\gamma_h)(\mu_m+\xi_m+\eta\tau)\\
&\times(\mu_m+\eta\tau+\sigma_m)+(\mu_h+\phi_h+\sigma_h)(\mu_h+\varepsilon_h+\pi_h)(\mu_m+\eta\tau+\sigma_m)\\
&+(\mu_h+\phi_h+\sigma_h)(\mu_h+\varepsilon_h+\pi_h)(\mu_m+\xi_m+\eta\tau)+(\mu_h+\phi_h+\sigma_h)\\
&\times(\mu_m+\xi_m+\eta\tau)(\mu_m+\eta\tau+\sigma_m)+(\mu_h+\varepsilon_h+\pi_h)(\mu_m+\xi_m+\eta\tau)\\
&\times(\mu_m+\eta\tau+\sigma_m)-(\mu_h+\gamma_h)\phi_h\varepsilon_h-(\mu_m+\xi_m+\eta\tau)\phi_h\varepsilon_h\\
&\left.-(\mu_m+\eta\tau)\phi_h\varepsilon_h\right]\lambda^2 + \left[(\mu_h+\gamma_h)(\mu_h+\phi_h+\sigma_h)(\mu_h+\varepsilon_h+\pi_h)\right.\\
&\times(\mu_m+\eta\tau+\sigma_m)+(\mu_h+\gamma_h)(\mu_h+\phi_h+\sigma_h)(\mu_h+\varepsilon_h+\pi_h)\\
&\times(\mu_m+\xi_m+\eta\tau)+(\mu_h+\gamma_h)(\mu_h+\phi_h+\sigma_h)(\mu_m+\xi_m+\eta\tau)\\
&\times(\mu_m+\eta\tau+\sigma_m)+(\mu_h+\gamma_h)(\mu_h+\varepsilon_h+\pi_h)(\mu_m+\xi_m+\eta\tau)\\
&\times(\mu_m+\eta\tau+\sigma_m)+(\mu_h+\phi_h+\sigma_h)(\mu_h+\varepsilon_h+\pi_h)(\mu_m+\xi_m+\eta\tau)\\
&\times(\mu_m+\eta\tau+\sigma_m)-(\mu_h+\gamma_h)(\mu_m+\eta\tau+\sigma_m)\phi_h\varepsilon_h-\left(\frac{\delta\beta_h(1-\nu)\psi_h}{\mu_h}\right)\\
&\left.\times\left(\frac{\delta\beta_m(1-\nu)\rho(1-\varphi)}{\mu_m}\right)\gamma_h\xi_m-(\mu_m+\xi_m+\eta\tau)(\mu_m+\eta\tau+\sigma_m)\phi_h\varepsilon_h\right]\lambda\\
&+\left[(\mu_h+\gamma_h)(\mu_h+\phi_h+\sigma_h)(\mu_h+\varepsilon_h+\pi_h)(\mu_m+\xi_m+\eta\tau)\right.\\
&\times(\mu_m+\eta\tau+\sigma_m)-(\mu_h+\gamma_h)(\mu_m+\xi_m+\eta\tau)(\mu_m+\eta\tau+\sigma_m)\phi_h\varepsilon_h\\
&\left.-\left(\frac{\delta\beta_h(1-\nu)\psi_h}{\mu_h}\right)(\mu_h+\varepsilon_h+\pi_h)\left(\frac{\delta\beta_m(1-\nu)\rho(1-\varphi)}{\mu_m}\right)\gamma_h\xi_m\right]=0
\end{aligned}
\tag{A1}
$$

$$
\begin{aligned}
&\lambda^5 + \left[(\mu_h+\gamma_h)+(\mu_h+\phi_h+\sigma_h)+(\mu_h+\varepsilon_h+\pi_h)+(\mu_h+\omega_h)\right.\\
&\left.+(\mu_m+\xi_m+\eta\tau)\right]\lambda^4 + \left[(\mu_h+\gamma_h)(\mu_h+\phi_h+\sigma_h)+(\mu_h+\gamma_h)\right.\\
&\times(\mu_h+\varepsilon_h+\pi_h)+(\mu_h+\gamma_h)(\mu_m+\xi_m+\eta\tau)+(\mu_h+\gamma_h)(\mu_m+\eta\tau+\sigma_m)\\
&+(\mu_h+\phi_h+\sigma_h)(\mu_h+\varepsilon_h+\pi_h)+(\mu_h+\phi_h+\sigma_h)(\mu_m+\xi_m+\eta\tau)\\
&+(\mu_h+\phi_h+\sigma_h)(\mu_m+\eta\tau+\sigma_m)+(\mu_h+\varepsilon_h+\pi_h)(\mu_m+\xi_m+\eta\tau)\\
&+(\mu_h+\varepsilon_h+\pi_h)(\mu_m+\eta\tau+\sigma_m)+(\mu_m+\xi_m+\eta\tau)(\mu_m+\eta\tau+\sigma_m)\\
&\left.-\phi_h\varepsilon_h\right]\lambda^3 + \left[(\mu_h+\gamma_h)(\mu_h+\phi_h+\sigma_h)(\mu_h+\varepsilon_h+\pi_h)+(\mu_h+\gamma_h)\right.\\
&\times(\mu_h+\phi_h+\sigma_h)(\mu_m+\xi_m+\eta\tau)+(\mu_h+\gamma_h)(\mu_h+\phi_h+\sigma_h)\\
&\times(\mu_m+\eta\tau+\sigma_m)+(\mu_h+\gamma_h)(\mu_h+\varepsilon_h+\pi_h)(\mu_m+\xi_m+\eta\tau)\\
&+(\mu_h+\gamma_h)(\mu_h+\varepsilon_h+\pi_h)(\mu_m+\eta\tau+\sigma_m)+(\mu_h+\gamma_h)(\mu_m+\xi_m+\eta\tau)\\
&\times(\mu_m+\eta\tau+\sigma_m)+(\mu_h+\phi_h+\sigma_h)(\mu_h+\varepsilon_h+\pi_h)(\mu_m+\eta\tau+\sigma_m)\\
&+(\mu_h+\phi_h+\sigma_h)(\mu_h+\varepsilon_h+\pi_h)(\mu_m+\xi_m+\eta\tau)+(\mu_h+\phi_h+\sigma_h)\\
&\times(\mu_m+\xi_m+\eta\tau)(\mu_m+\eta\tau+\sigma_m)+(\mu_h+\varepsilon_h+\pi_h)(\mu_m+\xi_m+\eta\tau)\\
&\times(\mu_m+\eta\tau)-(\mu_h+\gamma_h)\phi_h\varepsilon_h-(\mu_m+\xi_m+\eta\tau)\phi_h\varepsilon_h-(\mu_m+\eta\tau+\sigma_m)\\
&\times\phi_h\varepsilon_h\left.\right]\lambda^2 + \left[(\mu_h+\gamma_h)(\mu_h+\phi_h+\sigma_h)(\mu_h+\varepsilon_h+\pi_h)(\mu_m+\eta\tau+\sigma_m)\right.\\
&+(\mu_h+\gamma_h)(\mu_h+\phi_h+\sigma_h)(\mu_h+\varepsilon_h+\pi_h)(\mu_m+\xi_m+\eta\tau)+(\mu_h+\gamma_h)\\
&\times(\mu_h+\varepsilon_h+\pi_h)(\mu_m+\xi_m+\eta\tau)(\mu_m+\eta\tau+\sigma_m)+(\mu_h+\phi_h+\sigma_h)\\
&\times(\mu_h+\varepsilon_h+\pi_h)(\mu_m+\xi_m+\eta\tau)(\mu_m+\eta\tau+\sigma_m)-(\mu_h+\gamma_h)\\
&\times(\mu_m+\eta\tau+\sigma_m)\phi_h\varepsilon_h+(1-R_0)-(\mu_m+\xi_m+\eta\tau)(\mu_m+\eta\tau+\sigma_m)\\
&\times\phi_h\varepsilon_h\left.\right]\lambda+\left[(1-R_0)-(\mu_h+\gamma_h)(\mu_m+\xi_m+\eta\tau)(\mu_m+\eta\tau+\sigma_m)\phi_h\varepsilon_h\right]=0
\end{aligned}
\tag{A2}
$$